

NASA TECHNICAL NOTE



NASA TN D-4021

C.1

NASA TN D-4021

LOAN COPY: RETURN TO
AFWL (MAIL-2)
KIRTLAND AFB, N MEX



STING-SUPPORT INTERFERENCE ON
LONGITUDINAL AERODYNAMIC CHARACTERISTICS
OF CARGO-TYPE AIRPLANE MODELS
AT MACH 0.70 TO 0.84

by Donald L. Loving and Arvo A. Luoma

Langley Research Center

Langley Station, Hampton, Va.





0130811

NASA TN D-4021

STING-SUPPORT INTERFERENCE ON
LONGITUDINAL AERODYNAMIC CHARACTERISTICS
OF CARGO-TYPE AIRPLANE MODELS
AT MACH 0.70 TO 0.84

By Donald L. Loving and Arvo A. Luoma

Langley Research Center
Langley Station, Hampton, Va.

NATIONAL AERONAUTICS AND SPACE ADMINISTRATION

For sale by the Clearinghouse for Federal Scientific and Technical Information
Springfield, Virginia 22151 - CFSTI price \$3.00

STING-SUPPORT INTERFERENCE ON
LONGITUDINAL AERODYNAMIC CHARACTERISTICS
OF CARGO-TYPE AIRPLANE MODELS
AT MACH 0.70 TO 0.84

By Donald L. Loving and Arvo A. Luoma
Langley Research Center

SUMMARY

An investigation has been made in the Langley 8-foot transonic pressure tunnel to determine the effects of sting-support interference on the aerodynamic characteristics of models of cargo-type airplanes with fuselages having upswept aft ends. Special "live" and dummy stings and dorsal strut-support systems were utilized to cover a limited range of test variables from just below to just above the design-cruise lift condition of each particular model. Data were obtained from a conventional six-component balance and from extensive static-pressure surveys in the balance chamber, sting-fuselage cavity, and sting surfaces within the fuselage. Tests were performed at Mach numbers from 0.70 to 0.84 and at a Reynolds number of 19.7×10^6 per meter (6.0×10^6 per foot).

The results indicate that the sting-interference effects (sting tares), obtained through the use of a dorsal strut to support the models without and in the presence of a dummy sting, were of small magnitude. When tares were applied to the uncorrected lift-drag polar, the combination of the lift and drag tares resulted in differences between the uncorrected and corrected drag coefficient values at a given lift coefficient (net drag tares) of from 0 to 0.0004 in the design-cruise lift range.

INTRODUCTION

The determination of model-support interference-free results from information obtained during investigations of models in wind tunnels requires that support tares be evaluated and applied to the uncorrected data. In most high-speed wind-tunnel research involving body, wing-body, or complete airplane combinations, stings generally are used to support the models and the models have more or less axisymmetrical aft ends. As shown in references 1 to 4, methods are available not only for designing sting-support systems which will minimize the support interference, but also to ascertain, to some extent, the magnitude of the interference on the forces acting on such models.

In a recent wind-tunnel investigation of several cargo-type airplane configurations, the aft ends of the models, as for the full-scale counterparts, definitely were not axisymmetrical. At the juncture with a straight conventional sting support, the aft ends of the models incorporated a rather large degree of bottom upsweep. Because of the extreme nature of the upsweep angle, it was thought that the aft-end drag could be a critical part of the total drag and might be significantly affected by the presence of the sting. To make a proper assessment of the drag of such configurations, therefore, a careful evaluation of the sting-support interference (sting tare) was undertaken. To evaluate these sting-support tares, the models were supported on a dorsal (overhead) strut and tests were made both with and without a dummy rear sting present.

The sting-support interference study was made in the Langley 8-foot transonic pressure tunnel as part of a broader investigation of the longitudinal aerodynamic characteristics of three different proposed cargo-type airplanes. The sting-interference tests were conducted at Mach numbers from 0.70 to 0.84 and at angles of attack from -2° to 4° at a Reynolds number of 19.7×10^6 per meter (6.0×10^6 per foot). Data from these tests were used to determine the sting tares for an angle-of-attack range between approximately 0° and 3° to cover the design-cruise lift conditions of the different models. These data are shown herein in incremental form since it is not the purpose of this report to indicate the relative aerodynamic merits of the various models tested.

SYMBOLS

\bar{c}	mean aerodynamic chord of wing, meters
l	distance from balance center, positive when measured rearward, centimeters (fig. 8)
M	free-stream Mach number
p_l	local static pressure, newtons/meter ²
p	free-stream static pressure, newtons/meter ²
q	free-stream dynamic pressure, newtons/meter ²
S	total area of wing, meters ²
z	distance above or below sting center line, centimeters

α angle of attack of fuselage reference line, degrees

δ_h horizontal-tail deflection, positive when trailing edge is down, degrees

C_D drag coefficient, $\frac{\text{Drag}}{qS}$

C_L lift coefficient, $\frac{\text{Lift}}{qS}$

C_m pitching-moment coefficient, $\frac{\text{Pitching moment}}{qS\bar{c}}$

C_p local pressure coefficient, $\frac{p_l - p}{q}$

Model supported on live sting:

$$C_L' = C_L - (C_L)_{\text{at } C_{D,\min}}$$

$$C_D' = C_D - C_{D,\min}$$

$$C_m' = C_m - (C_m)_{\text{at } C_{D,\min}}$$

Model supported on dorsal strut; dummy sting either on or off:

$$C_L'' = C_L - C_{L,K}$$

$$C_D'' = C_D - C_{D,K}$$

$$C_m'' = C_m - C_{m,K}$$

where $C_{L,K}$, $C_{D,K}$, and $C_{m,K}$ are arbitrary constants having the same value for each set of two runs used to determine tares.

$$C_{L,\text{sting tare}} = (C_L'')_{\text{dummy sting on}} - (C_L'')_{\text{dummy sting off}}$$

$$C_{D, \text{sting tare}} = (C_{D''})_{\text{dummy sting on}} - (C_{D''})_{\text{dummy sting off}}$$

$$C_{m, \text{sting tare}} = (C_{m''})_{\text{dummy sting on}} - (C_{m''})_{\text{dummy sting off}}$$

Subscript:

min minimum

APPARATUS

Test Facility

The Langley 8-foot transonic pressure tunnel is a closed-circuit, continuous-flow wind tunnel capable of operating at Mach numbers between 0.2 and 1.3. The total pressure of the air in the tunnel can be varied from a minimum value of about 0.25 atmosphere at all test Mach numbers to a maximum value of about 1.5 atmosphere at transonic Mach numbers and about 2 atmospheres at Mach numbers of 0.4 and less. The location in the tunnel of the balance center of each of the models and the basic features of the conventional sting-support system in the region of the test section, as adapted to this investigation, are indicated in figure 1. The ratio of model wing span to tunnel width was about 0.7. Normally, much smaller models are tested in a facility of this size. However, it has been shown in references 5 and 6 that large-scale models, which permit high values of model Reynolds numbers, can be tested at subsonic speeds in relatively small transonic tunnels, such as the Langley 8-foot transonic pressure tunnel, and that a high level of confidence can be placed in the results of such tests.

Photographs of a typical complete model configuration installed on the conventional sting support in the tunnel are shown as figures 2(a) and 2(b).

Model Configurations

Basic details of the complete configurations of the three cargo-type scale models (designated models A, B, and C) used in the investigation are presented in figures 3(a), 3(b), and 3(c), respectively. Each of the models featured a sweptback wing located at the top of the fuselage, and four turbofan engine nacelles mounted on pylons under the wing. The turbofan engine nacelles were designed to have the proper inlet geometry and internal mass flow.

Models A and B incorporated a conventional vertical tail with a horizontal tail mounted on the side of the fuselage aft end. Model C utilized a "T" tail arrangement with the horizontal tail mounted on top of the vertical tail.

For this sting-tare evaluation, the most important feature of the models that had to be considered was the aft end geometry. (See fig. 4.) As indicated in figure 4, the fuselage aft-end upsweep angle varied from approximately 19° for model A to 15° for model C. The afterbody fineness ratios, based on the fuselage cross-sectional height at the beginning of the bottom upsweep and the aft-end length from this point to the afterbody tip, were approximately 2.8, 4.0, and 3.9 for models A, B, and C, respectively.

Model Support Systems

Various model supports used in the investigation of the aerodynamic characteristics as well as the sting-support interference are shown in the drawings of figures 5 and 6, and the photographs of figures 2 and 7.

The details of the model supports were determined mainly in an attempt to minimize sting-interference effects for all the models. No attempt was made to develop experimentally a particular support system that would be completely devoid of interference effects.

Sting support.- As mentioned, the principal support system selected for the broad investigation was the straight conventional sting, which is referred to herein as the "live" sting. The method of attachment of this sting to the balance within the models is shown in figure 5. The size and shape of the live sting was determined by consideration of a reasonable restriction to the bending deflections in addition to the usual load-stress requirements. The live sting was designed for a maximum allowable deflection of 1.5 centimeters at the balance center, based on the maximum anticipated design-cruise load condition for the models to be tested. The reason for imposing this restriction was the requirement that the sting be stiff enough to allow a straight, duplicate (but dummy) sting to be positioned properly in the fuselage-sting cavity. Proper positioning required that the gaps around the dummy sting be as near as possible to those experienced by the live sting with the model under load corresponding to the design-cruise lift range. An oval-type shape, as may be detected in the photographs of figures 2 and 7 and as shown in figures 5 and 6, was selected to make the stings more streamlined to the flow in the vertical direction. This approach was taken in order to minimize aerodynamic interference effects at angle of attack. It also was considered that such a shape would be relatively straightforward to fabricate. The constant-section portion of the sting behind the base of the fuselages was about five times the average fuselage aft-end diameter to minimize any interference of the sting flare on the model aerodynamic forces (ref. 1). The sting flare with a total angle of approximately 11° in planform and 15° in side view resulted from the addition of a fairing followed by a strengthening collar over the junction between the sting and downstream portion of the tunnel support system. (See fig. 1 and the photographs in fig. 2.) A similarly shaped fairing covered the components of the dummy-sting

coupling. (See fig. 6 and the photographs of fig. 7.) Additional stiffness to the overall support systems was provided by diagonal guy wires (maintained under preset tension) attached to each side of the sting-support barrel at the angle-of-attack pivot point. (See figs. 1, 2(a), and 7.)

Electrical fouling indicators attached either to the model supports or to the models were used to ensure that the support systems did not come in direct contact with the models for both wind-on and wind-off test conditions except through attachment to the balance.

Dorsal-strut support.- A dorsal strut was used to support the models in the tunnel when they were not attached to the live sting. (See figs. 5 to 7.) This strut entered the top of each fuselage with the leading edge about 15 centimeters downstream from the wing-fuselage trailing-edge juncture to minimize the influence of the strut on the flow over the wing. The streamwise cross sections of the strut were NACA 65A008 airfoil sections. A short vertical section of the strut protruded above the top of each fuselage just enough to prevent the sweptback trailing-edge portion of the strut from fouling on the fuselage when the balance deflected under load. A very low restraining-force sponge-rubber seal was provided around the fuselage cut-out to inhibit flow through the gap and thus to ensure a uniform air pressure within the balance chamber. Above the short vertical section of the strut, the strut leading edge was swept back 41.70° and had a taper ratio of approximately 0.67. The section thickness, airfoil profile, and sweepback angle of the strut were selected to provide a relatively high critical speed and yet be able to sustain the anticipated loads on the support system, and to center any side loads that might occur as close as possible to the torsional axis of the strut. The lower edge of the overhead support for the dorsal strut was located approximately two body diameters above the top of the fuselages. The method of attachment of the dorsal-strut support to the balance is shown in figure 5. The model is shown without and with a dummy sting. When supported by the strut, models A and B were without vertical tails but with horizontal tails on. Model C was without both vertical and horizontal tails. The vertical tails on all three models would have physically interfered with the dorsal strut because of their size and location. In the case of model C, as mentioned earlier, the horizontal tail was located on top of the vertical tail. Removing the vertical tail, therefore, resulted also in the elimination of the horizontal tail for this particular model.

Dummy sting.- The size and shape of the dummy sting were identical to those of the live sting, as shown in figure 5, except that the dummy sting terminated within a fuselage cavity. The dummy sting was not attached to the balance, nor did it touch any part of the model. The fuselage cavity was made sufficiently deep to assure a uniformity of air pressure over the forward end of the dummy sting and the cavity forward bulkhead. The

bulkhead and walls of the fuselage cavity were sealed to prevent any leakage of air between the cavity and the model balance chamber.

Instrumentation

A six-component, internal, strain-gage balance was used to measure forces and moments during the investigation. Static pressures were measured by differential transducers in scanners connected to various pressure orifices. Model angle of attack was measured by a strain-gage attitude indicator located in the model nose.

PROCEDURES, CORRECTIONS, AND ACCURACY

General

The models were tested for the sting-tare evaluation at Mach numbers from 0.70 to 0.84 at a constant Reynolds number of 19.7×10^6 per meter (6.0×10^6 per foot). Over the Mach number range, the total pressure ranged from about 15.8×10^4 to 17.4×10^4 newtons/m² (3295 to 3635 psf) and the total temperature was maintained at 49° C (120° F).

Tunnel conditions were held constant at each Mach number while the angle of attack was varied. The angle-of-attack range was from -2° to 4°.

Transition strips of carborundum grit 0.254 centimeter (0.10 in.) wide were placed near the leading edge of the wing, horizontal and vertical tails, pylons, nacelles, and nose of the fuselage. Selection of the grit size to cause transition was based on the information in reference 7 and on the results of initial runs of the present investigation when the effects on drag of transition grit size were determined.

Static Pressures

A number of static pressures were measured during the test at identical locations on the top, side, and bottom of the live and dummy stings within the area of the fuselage-sting cavity. Static pressures were measured in the model balance chamber and on the forward end of the dummy sting. For two of the models (models A and B), static pressures on the top wall of the cavity were obtained. The longitudinal variation of static pressures measured for the dummy sting present with models A, B, and C are shown in figures 8(a), 8(b), and 8(c), respectively, for a representative Mach number of 0.80 and an angle of attack of 1°. At the top of each figure is a sketch of each model afterbody; points on sketch correspond to the abscissa scale. The dummy sting is located in the fuselage-sting cavity. The gaps shown are initial no-load gaps and do not represent

actual clearances for the model under load. The locations of the orifices are indicated by the solid dots. Orifices on the forward end of the dummy sting are indicated in the end-view sketch.

The purpose of the static pressures being measured in the fuselage-sting cavity was to adjust the aerodynamic coefficients to a condition of free-stream static pressure in the cavity for the configurations in the presence of either the live or dummy stings. For the live sting, the axial-force coefficient was adjusted by subtracting the base axial-force coefficient computed by using the balance chamber pressure and the cross-sectional area of the fuselage-sting cavity. Similarly, for the dummy sting, the average of the static pressures on the forward end of the dummy sting and the cavity cross-sectional area were used. Limited tests showed that the static pressures on the cavity walls were identical to those acting on the stings at the same longitudinal location. The normal-force adjustment, therefore, was accomplished by integrating longitudinal distributions of pressure coefficients within the fuselage-sting cavity, such as are shown in figure 8. The increments in normal-force coefficient resulting from these integrations were based on the top and bottom planform areas of the cavity and applied to the balance normal-force coefficient. The pitching-moment coefficient adjustment involved the use of the integrated normal-force increment, the cavity planform areas, and the moment-arm length from the centroid of these areas to 0.25-percent mean aerodynamic chord.

It was not necessary to adjust the forces for the model supported by the dorsal strut alone since the fuselage aft end for this case was completely closed in, as it would be on the actual airplane. The static pressures for the live and dummy stings also were compared directly and the data showed that within the measuring accuracy of the instrumentation, the pressures on the stings and on the walls within the fuselage cavity were essentially the same. Since these pressures were the same for the live and dummy stings, it may be concluded that the effects of the live and the dummy stings on the pressures over the exterior surface of the fuselage aft ends were essentially the same.

Sting Tares

The interference of the sting on the model longitudinal aerodynamic forces and moments, herein also referred to as sting tares, were obtained by the procedure outlined in figure 9. The aerodynamic results for the model supported by the dorsal strut (tare run B) were subtracted from the aerodynamic results for the model supported by the same strut with the model in the presence of the dummy sting (tare run A); and this difference is the sting tare. These sting tares, in turn, were used to adjust the live sting aerodynamic results (normal run) to sting-interference-free data (model force).

Before testing each model with the dummy sting in place (tare run A), the configuration mounted on the live sting was statically loaded at the previously determined center-of-pressure location for the normal force associated with the design-cruise lift conditions. The fuselage-sting cavity clearances above and below the live sting and the angle of the sting center line relative to the model center line were measured and recorded. These clearances and sting angles were duplicated when the dummy sting was fixed in position and the design load was applied for each of the three models tested.

Accuracy of Measurements

The uncertainties associated with the various tunnel conditions and aerodynamic coefficients presented in this report are listed for a Mach number range from 0.70 to 0.84 at a Reynolds number of 19.7×10^6 per meter (6.0×10^6 per foot).

M	±0.003
α , deg	±0.05
C_L	±0.004
C_D	±0.0003
C_m	±0.0015
C_p	±0.005

Since the data were determined principally from single sample measurements (a few re-runs and repeat data points were made), the uncertainties were estimated upon the accuracy of instrumentation components. The uncertainties in force and moment coefficients include the errors associated with balance zero shifts and calibration curve fits.

The angle of attack was adjusted for tunnel-wall—model lift interference such that $\Delta\alpha = 0.10C_L$, where $\Delta\alpha$ is in degrees. Even so, the adjustment was small. For instance, for a cruise lift coefficient of 0.5, the wall-lift interference would amount to a reduction in angle of attack of only 0.05° , which is within the measuring accuracy of the test instrumentation.

RESULTS AND DISCUSSION

The data were reduced to aerodynamic coefficients referenced to a wind-axis coordinate system with the moment reference point located longitudinally at a fuselage station coincident with the 25-percent point of the wing mean aerodynamic chord, and vertically at waterline stations 0.00 centimeter (0.000 in.), 6.26 centimeters (2.463 in.), and 3.80 centimeters (1.495 in.) above the fuselage reference plane for models A, B, and C, respectively.

The aerodynamic coefficients for the tare runs (tare runs A and B) and also the data uncorrected (normal run) and corrected (model force) for the tares are presented in incremental form. These increments were obtained for the various comparable combination runs by subtracting the value of lift, drag, and pitching-moment coefficient at the test condition corresponding to minimum-drag coefficient from the absolute values of the coefficients. (See fig. 10 and the section "Symbols.") The angle of attack, however, was not adjusted during this axes translation.

Representative data ($M = 0.80$) from which sting tares for the three models were obtained are shown in figures 11, 12, and 13 as the variation of lift, drag, and pitching-moment coefficient with angle of attack. The data for models A and B were obtained for the configurations with the horizontal tail set at two different deflections. The data for model C are for the model without horizontal tail as explained in the section "Support Systems."

Even though sting-tare information was specifically required only for the angle-of-attack range between approximately 0° and 3° to cover the cruise lift conditions, data from -2° to 0° also were obtained and are included in the figures since they proved helpful in fairing the data.

Sting Tares

The sting tare values obtained from the tare runs are shown in figures 14(a), 14(b), and 14(c), for models A, B, and C, respectively, again as a function of angle of attack and for all the Mach numbers for which tare runs were made. The Mach number range used for the different models reflects the cruise-speed range for which the various configurations were designed. The horizontal-tail settings were chosen with consideration of trim conditions for models A and B. In the case of model C, the tail-off tare was used for tail-on deflection angles for this particular model to cover trim conditions.

The general conclusion gained from an examination of these sting tare values is that they are reasonably small in magnitude compared with the values of the uncorrected data.

For the entire Mach number and angle-of-attack range used in the sting-interference evaluation, the sting tare values varied from 0 to 0.0200 in lift coefficient, -0.0005 to 0.0016 in drag coefficient, and -0.0190 to 0.0035 in pitching-moment coefficient. At a representative cruise Mach number of 0.80 and approximate cruise angles of attack of 0.5° for model A ($\delta_h = -0.1^\circ$), 2° for model B ($\delta_h = 0.2^\circ$), and 1° for model C (horizontal tail off), the sting tare values were 0.0135, 0.0200, and 0 in lift coefficient; 0.0004, 0.0010, and 0.0005 in drag coefficient; and -0.0240, -0.0332, and 0.0020 in pitching-moment

coefficient, respectively. These results satisfied the objective that the support-interference effects be small and it also justified the design philosophy used for the support systems.

For these representative test conditions the sting drag tare for each model has a positive value. Thus, for design and near-design angle-of-attack conditions, the drag, adjusted for base pressure, was greater with the sting in place than with the sting removed and the aft end completely closed in, as for the actual airplane.

Generally, the variations of sting tares with test conditions are an irregular but small effect of change of Mach number, a gradual sting drag tare increase with increase in angle of attack, and a decrease in the sting drag tare for models A and B, and more positive sting pitching-moment tares for model B with more negative horizontal-tail deflection. When models A and B sting tares (figs. 14(a) and 14(b)) for horizontal-tail deflections near 0° are compared with model C sting tares (fig. 14(c)), the values for the latter configuration are shown to be the smallest.

Figure 15 shows the manner in which the sting lift, drag, and pitching-moment tares are applied to correct the uncorrected (normal run) test points. In the variation of the angle of attack with lift coefficient, it may be noted that it is necessary to make only one correction to the data; whereas in the variation of the drag coefficient and pitching-moment coefficient with lift coefficient, two corrections to the data are necessary.

In figures 16, 17, and 18 are shown the uncorrected variations with lift coefficient of angle of attack, drag coefficient, and pitching-moment coefficient for the models mounted on the live sting. The data for models A and B are for two horizontal-tail deflections; the data for model C are for horizontal tail off and one tail-on deflection. These data corrected for the sting tares by the method outlined in figure 15 also are included in figures 16 to 18. It may be noted that in the angle-of-attack range for design-cruise lift, the slopes of the lift curve ($dC_L/d\alpha$) and the stability curve (dC_m/dC_L) are not much different whether uncorrected or corrected for sting tares. This condition reflects the small effect of angle of attack on the sting lift and pitching-moment tares shown in figure 14. There is a displacement between the uncorrected and corrected lift and stability curves which draws attention to possible effects of the sting tares on trim.

Net Drag Tare

In the lift-drag polar plots shown in figures 15 to 18, the difference between the uncorrected and corrected drag coefficients at a constant lift coefficient may be considered as a net drag tare. The values of these net drag tares are of considerably greater significance than the magnitude of the previously discussed sting drag tares for a given angle of attack. It may be observed from figure 15 that when the sting lift and

drag tares are applied to the lift-drag polar, the difference between the uncorrected and corrected drag coefficient data at a given lift coefficient (net drag tare) can be substantially different from the sting drag tare. An examination of the net drag tares at the cruise conditions ($\alpha = 0^\circ$ to 3°) for all three models indicated that the values are less than the sting drag tares. For some cases, the application of the sting lift and drag tares actually resulted in a net drag tare of zero. For example, from the data in figure 14(a) at near design-cruise conditions of $M = 0.82$, and $\alpha = 0.5^\circ$ for model A with a horizontal-tail deflection of -0.1° , a sting lift tare of 0.0110 and a sting drag tare of 0.0006 were evaluated. When these two corrections are made to the lift-drag polar of figure 18(b), the net change in drag coefficient (net drag tare) is 0. For model B at near design-cruise conditions of $M = 0.82$, $\alpha = 2^\circ$, and $\delta_h = 0.2^\circ$, the net drag tare is 0.0004 (fig. 17(b)). Similarly, for model C at $M = 0.775$, $\alpha = 1^\circ$, and $\delta_h = 0^\circ$, the net drag tare is 0.0002 (fig. 18(g)).

CONCLUDING REMARKS

The results of an evaluation of the sting-interference effects on the longitudinal aerodynamic characteristics of cargo-type airplane models supported by a dorsal strut both without and with a dummy sting indicate that the sting tare values for constant angle of attack were small in magnitude compared with the values for the uncorrected data. When applied to the lift-drag polar, the combination of the sting lift and drag tares tended to cancel each other. The net drag tares for a given lift coefficient in the design-cruise lift range varied from 0 to 0.0004.

Langley Research Center,
National Aeronautics and Space Administration,
Langley Station, Hampton, Va., March 30, 1967,
126-13-01-39-23.

REFERENCES

1. Love, Eugene S.: A Summary of Information on Support Interference at Transonic and Supersonic Speeds. NACA RM L53K12, 1954.
2. Tunnell, Phillips J.: An Investigation of Sting-Support Interference on Base Pressure and Forebody Chord Force at Mach Numbers From 0.60 to 1.30. NACA RM A54K16a, 1955.
3. Lee, George; and Summers, James L.: Effects of Sting-Support Interference on the Drag of an Ogive-Cylinder Body With and Without a Boattail at 0.6 and 1.4 Mach Number. NACA RM A57I09, 1957.
4. Cahn, Maurice S.: An Experimental Investigation of Sting-Support Effects on Drag and a Comparison With Jet Effects at Transonic Speeds. NACA Rept. 1353, 1958. (Supersedes NACA RM L56F18a.)
5. Wright, Ray H.; and Barger, Raymond L.: Wind-Tunnel Lift Interference on Sweptback Wings in Rectangular Test Sections With Slotted Top and Bottom Walls. NASA TR R-241, 1966.
6. Bielat, Ralph P.; Luoma, Arvo A.; and Daugherty, James C.: Drag Measurements From Different Wind Tunnels. NASA TM X-1271, 1966.
7. Braslow, Albert L.; and Knox, Eugene C.: Simplified Method for Determination of Critical Height of Distributed Roughness Particles for Boundary-Layer Transition at Mach Numbers From 0 to 5. NACA TN 4363, 1958.

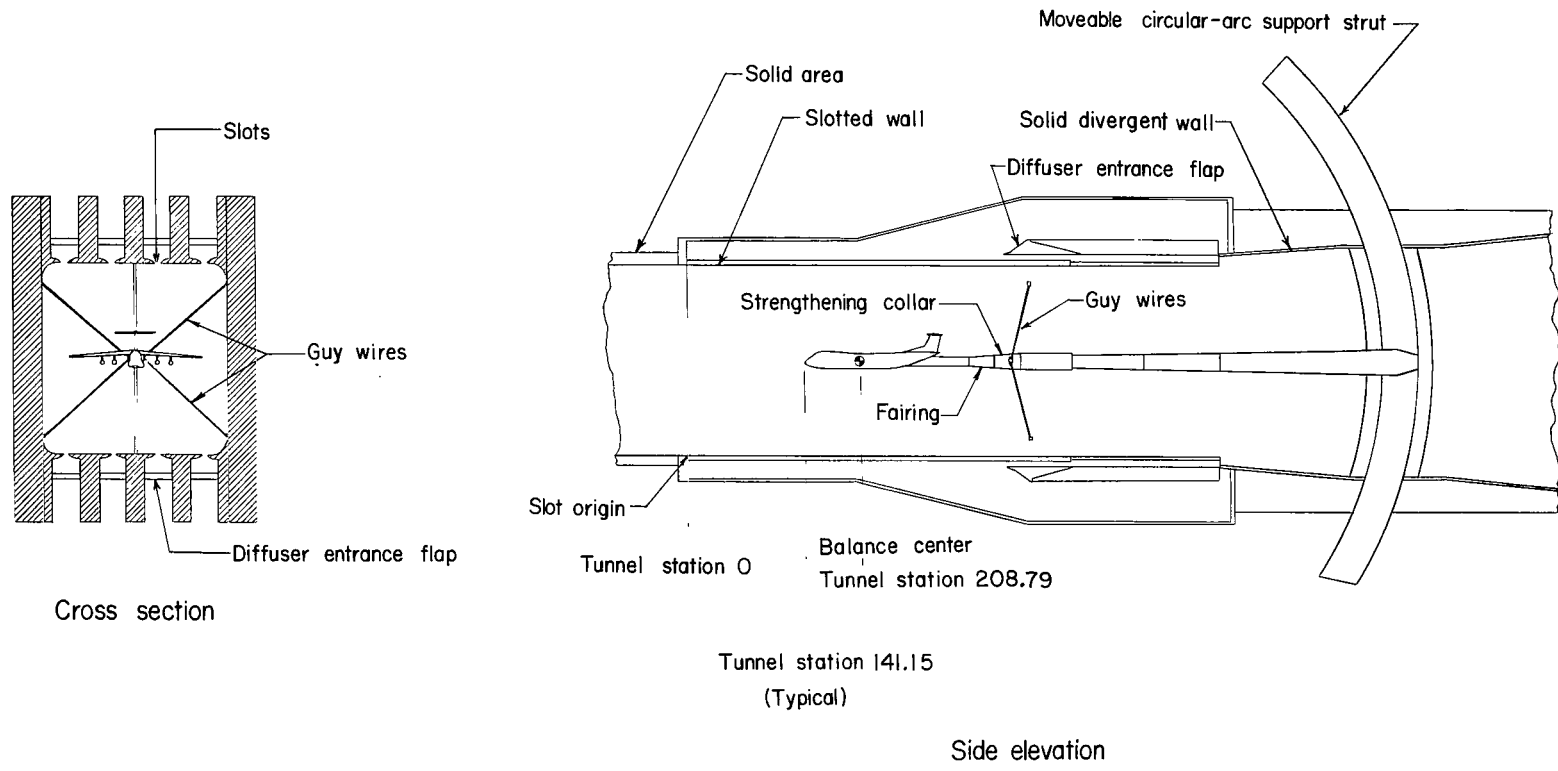
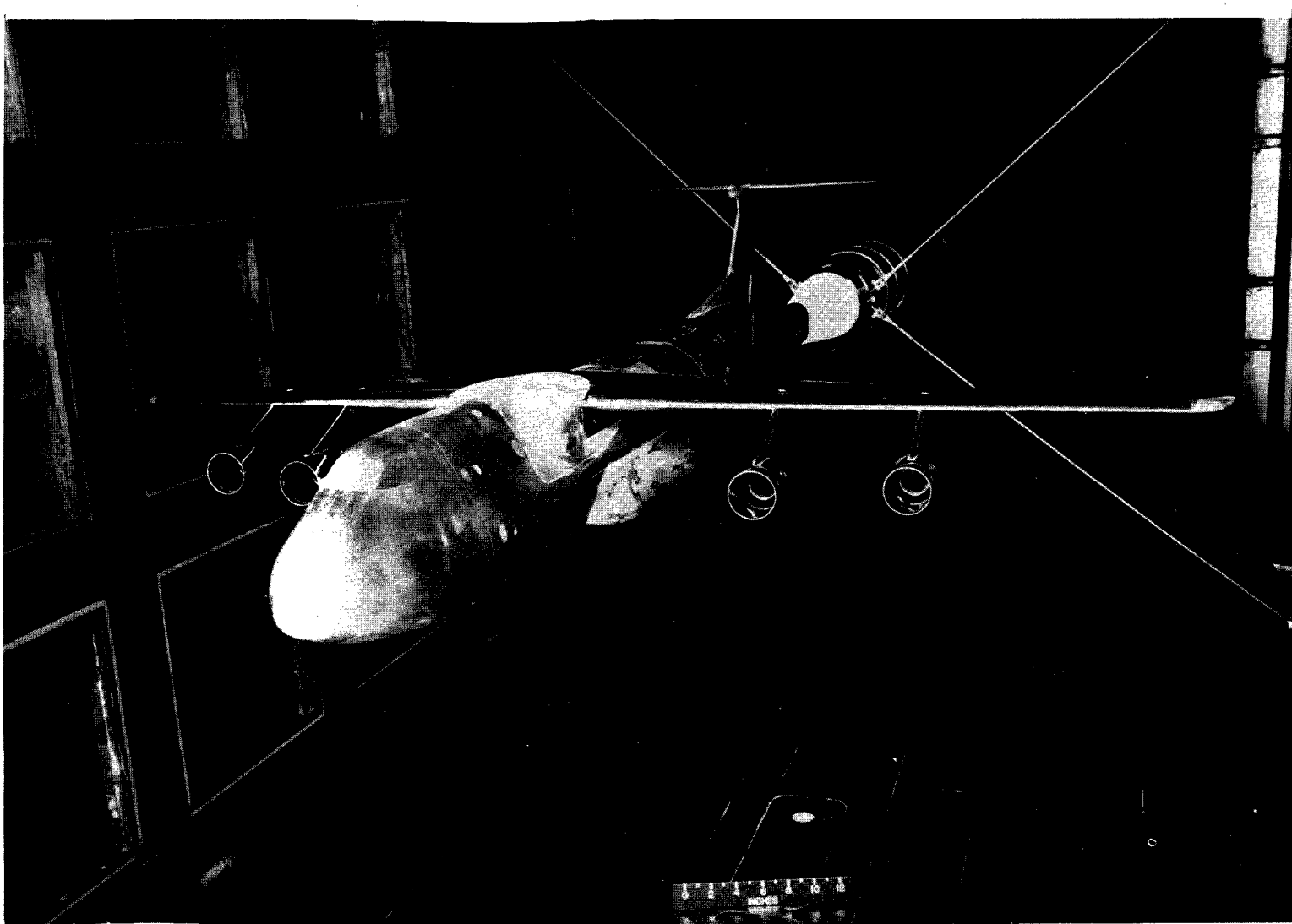


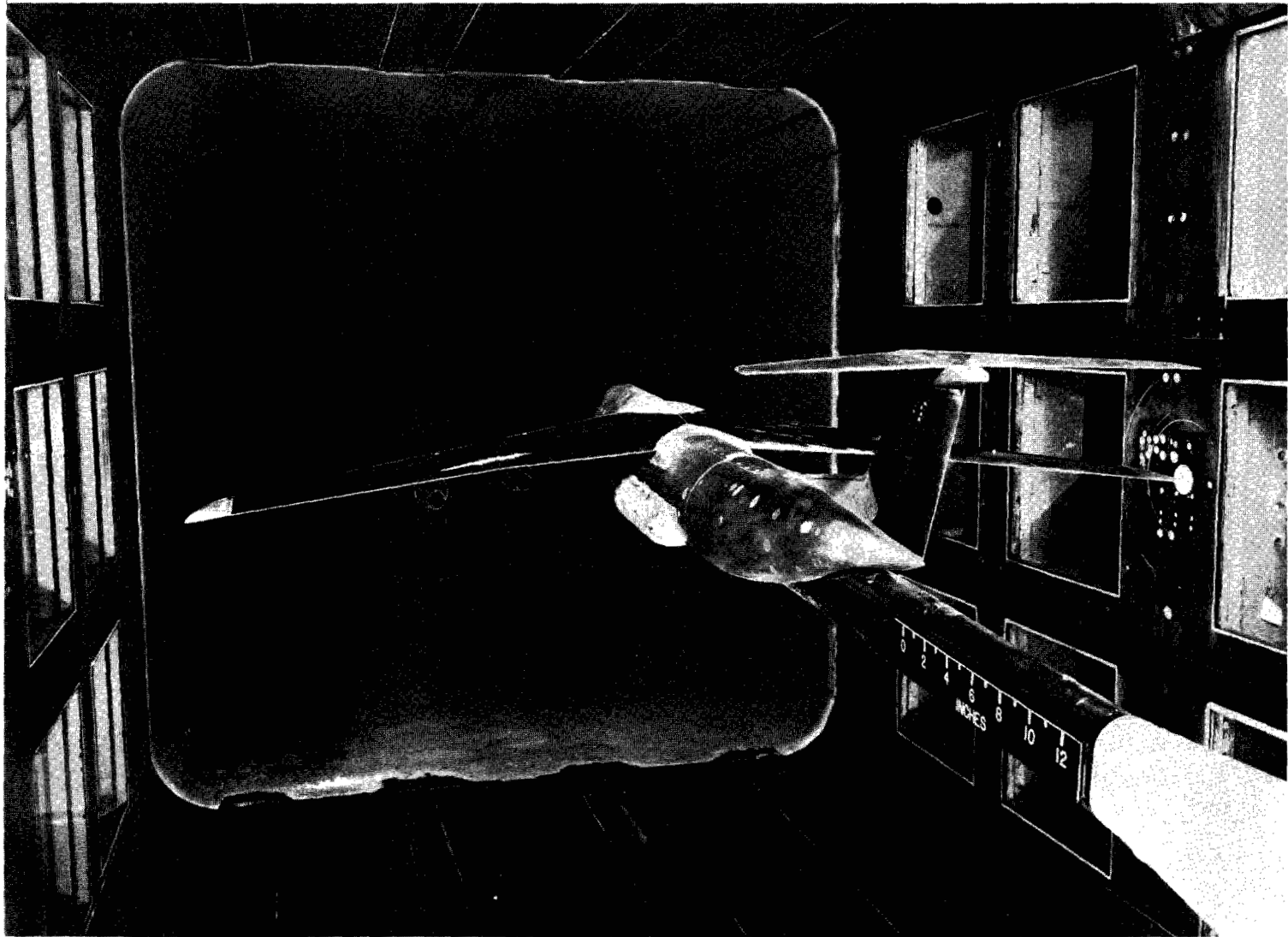
Figure 1.- Cargo-type airplane model installation in the Langley 8-foot transonic pressure tunnel. All dimensions are in centimeters.



(a) Front quarter view.

L-65-1900

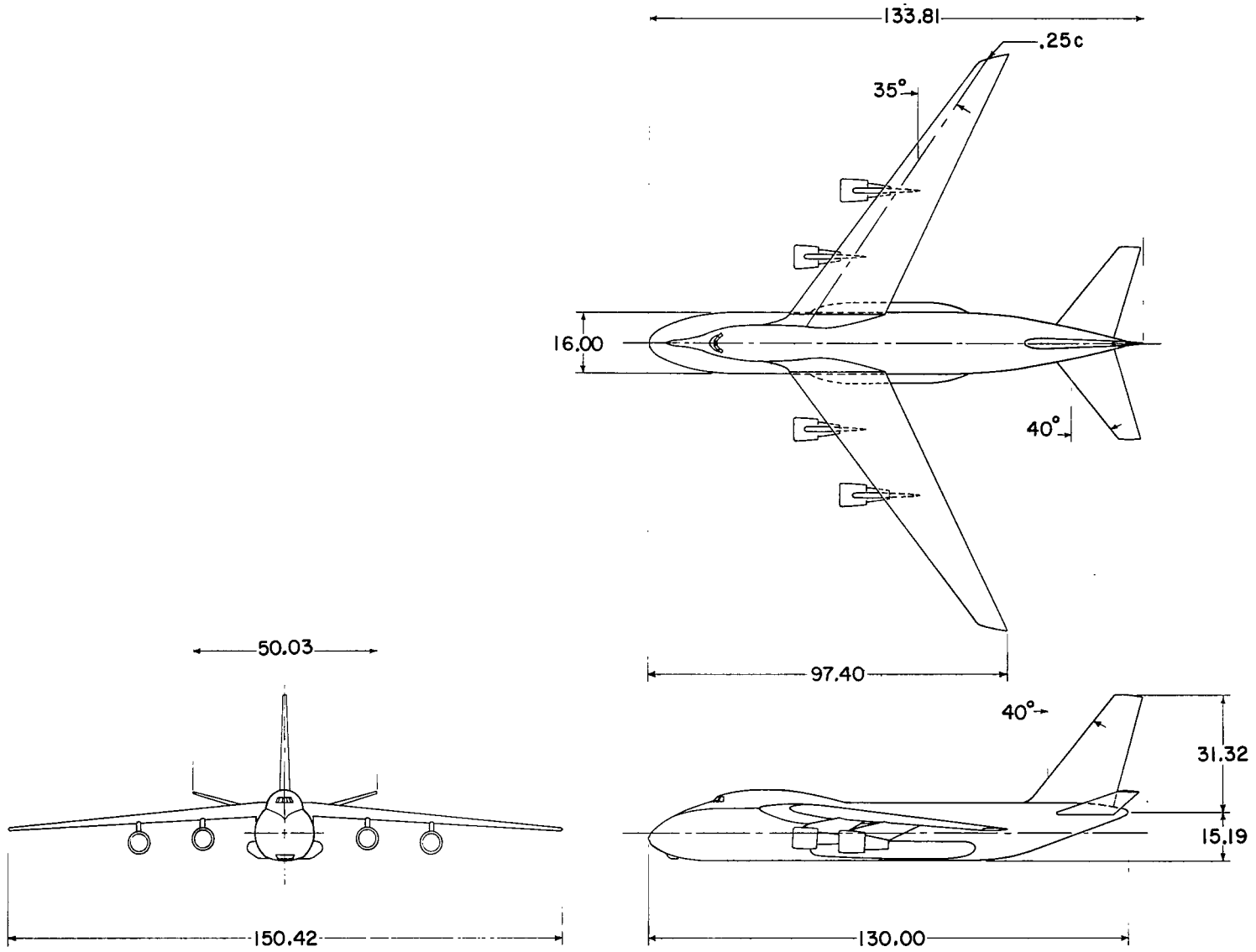
Figure 2.- Photograph of typical cargo-type airplane model supported by conventional sting in test section.



(b) Rear quarter view.

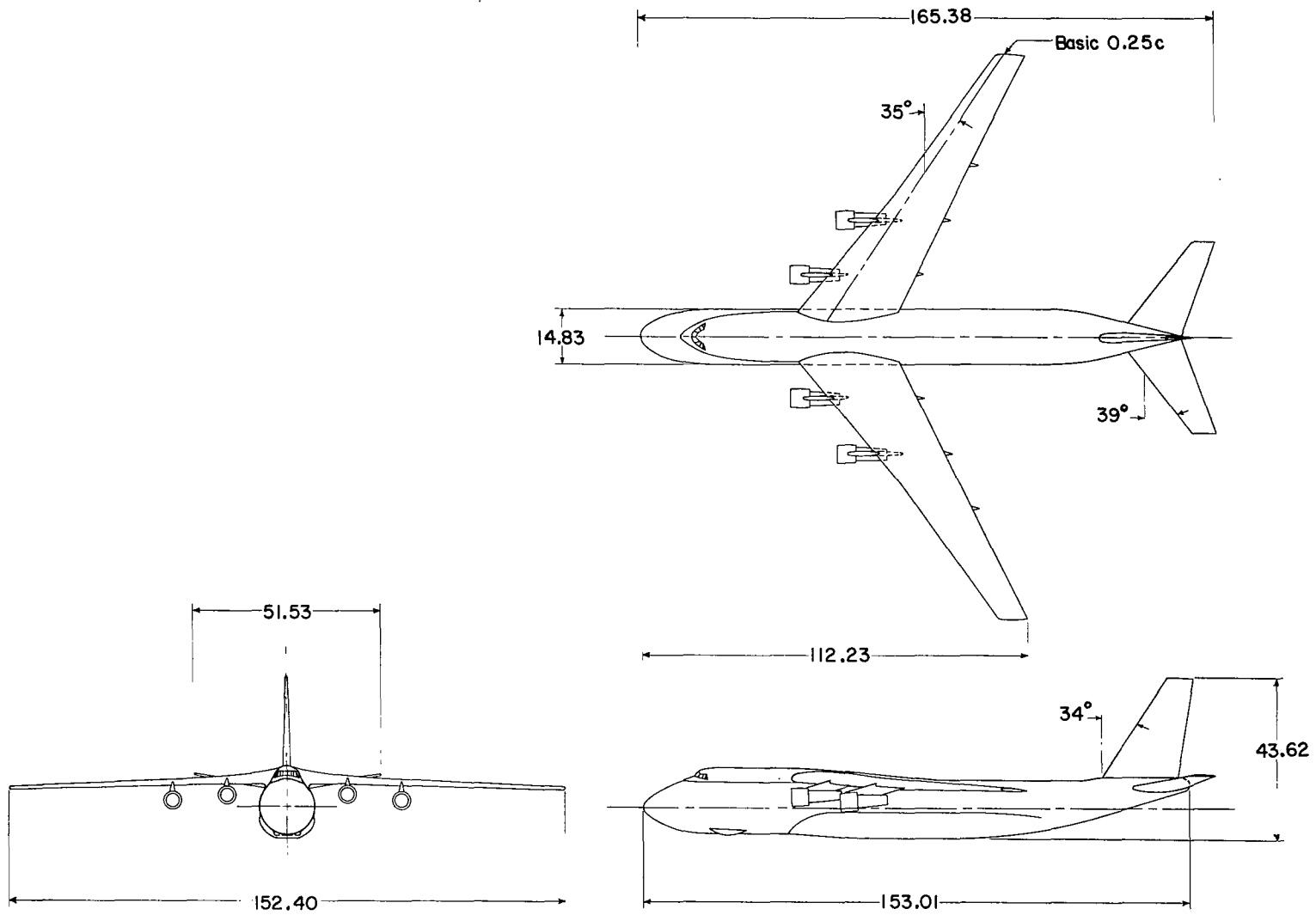
L-65-1896

Figure 2.- Concluded.



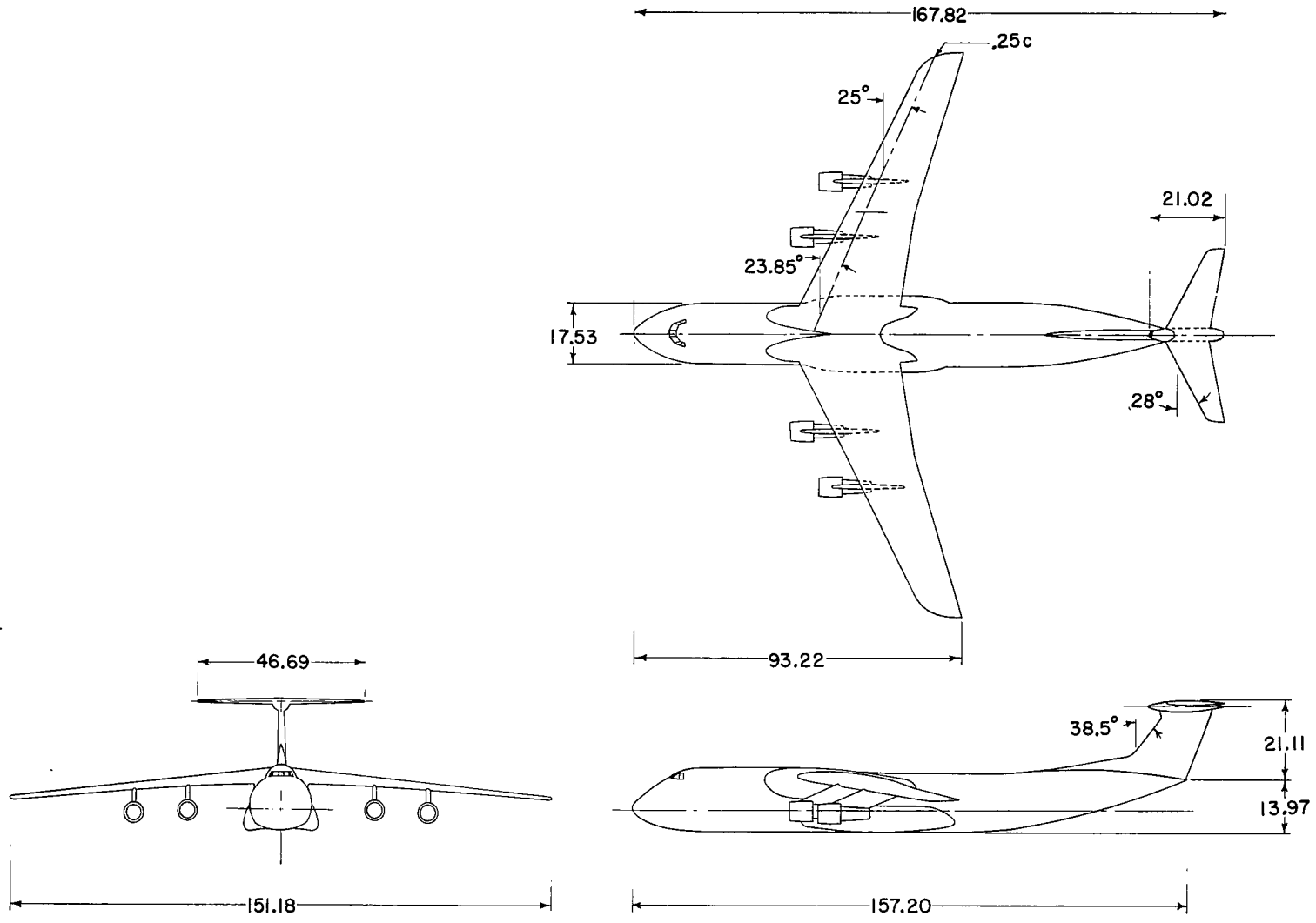
(a) Model A.

Figure 3.- Basic details of models tested. All dimensions are in centimeters.



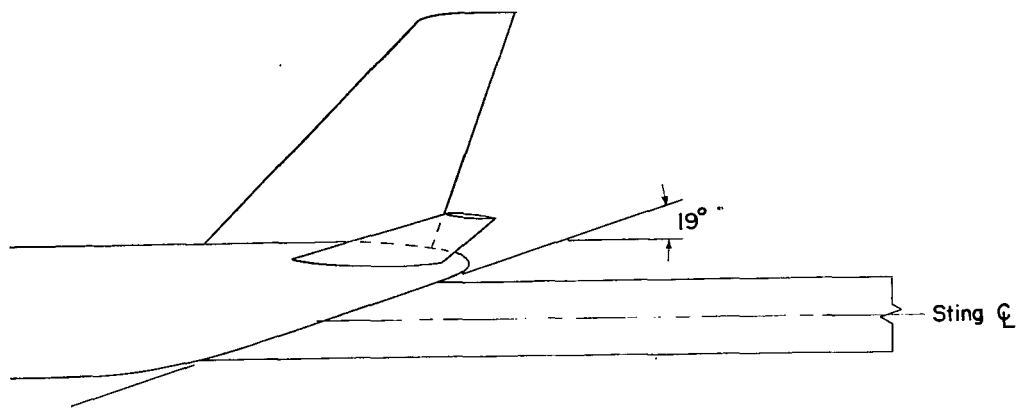
(b) Model B.

Figure 3.- Continued.

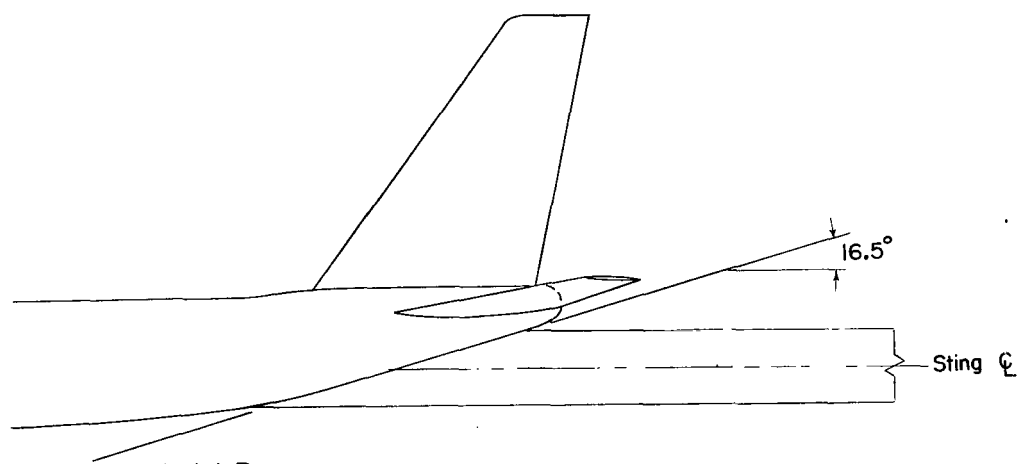


(c) Model C.

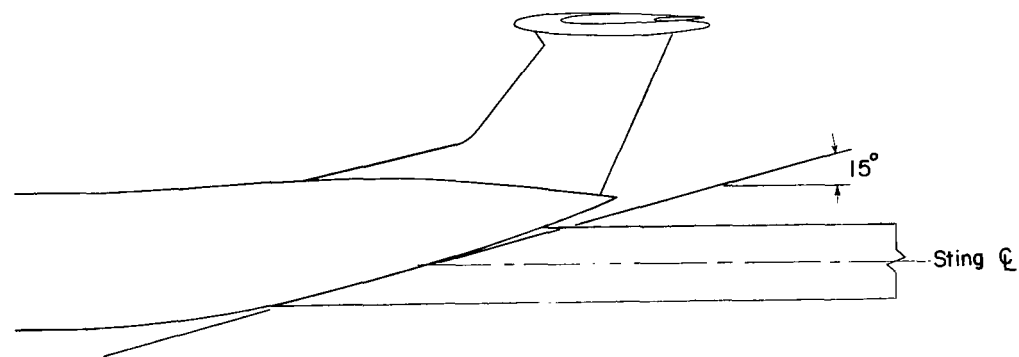
Figure 3.- Concluded.



Model A



Model B



Model C

Figure 4.- Aft-end geometry of models.

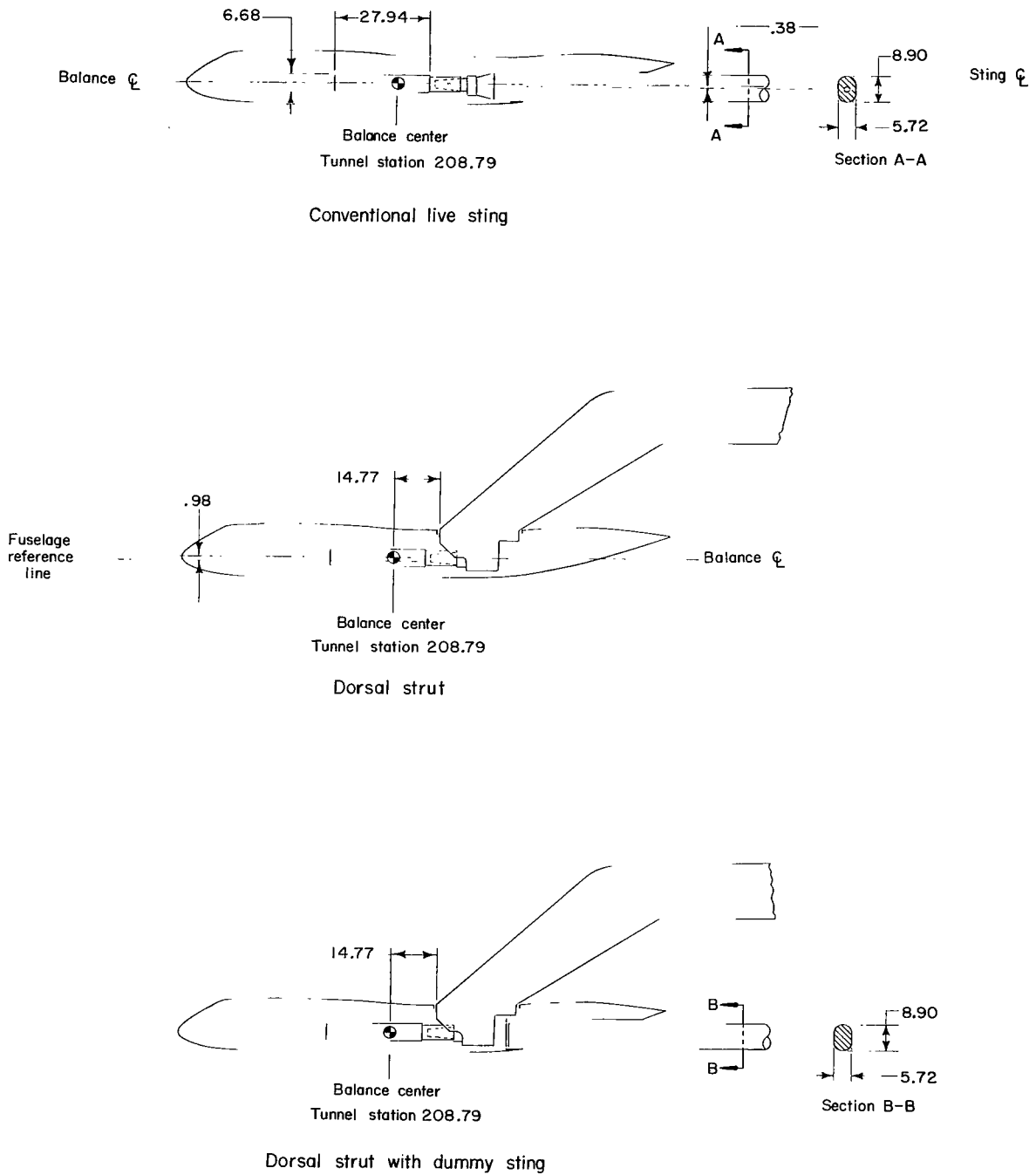


Figure 5.- Model-support systems used and method of attachment to balance. All dimensions are in centimeters.

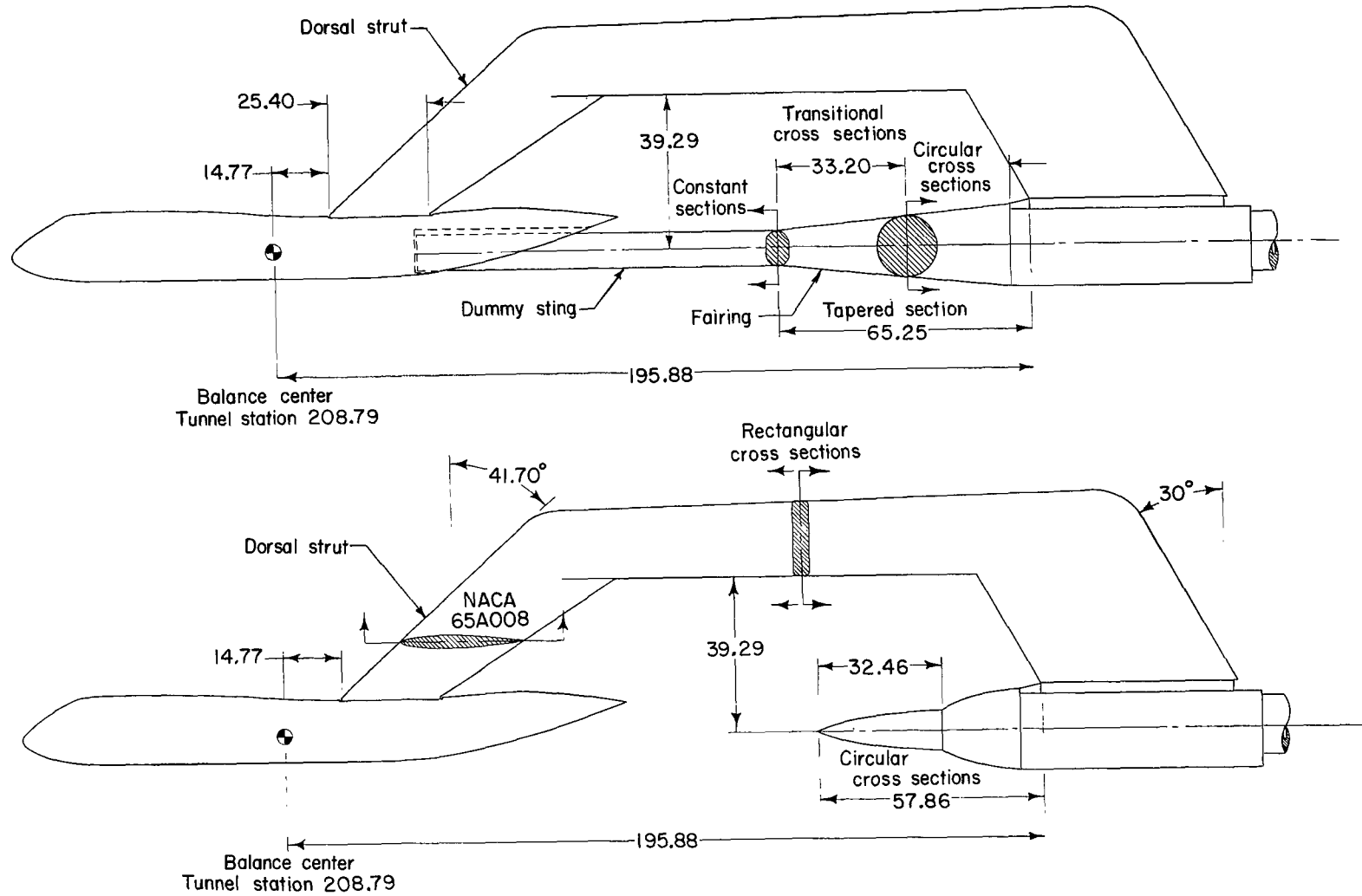
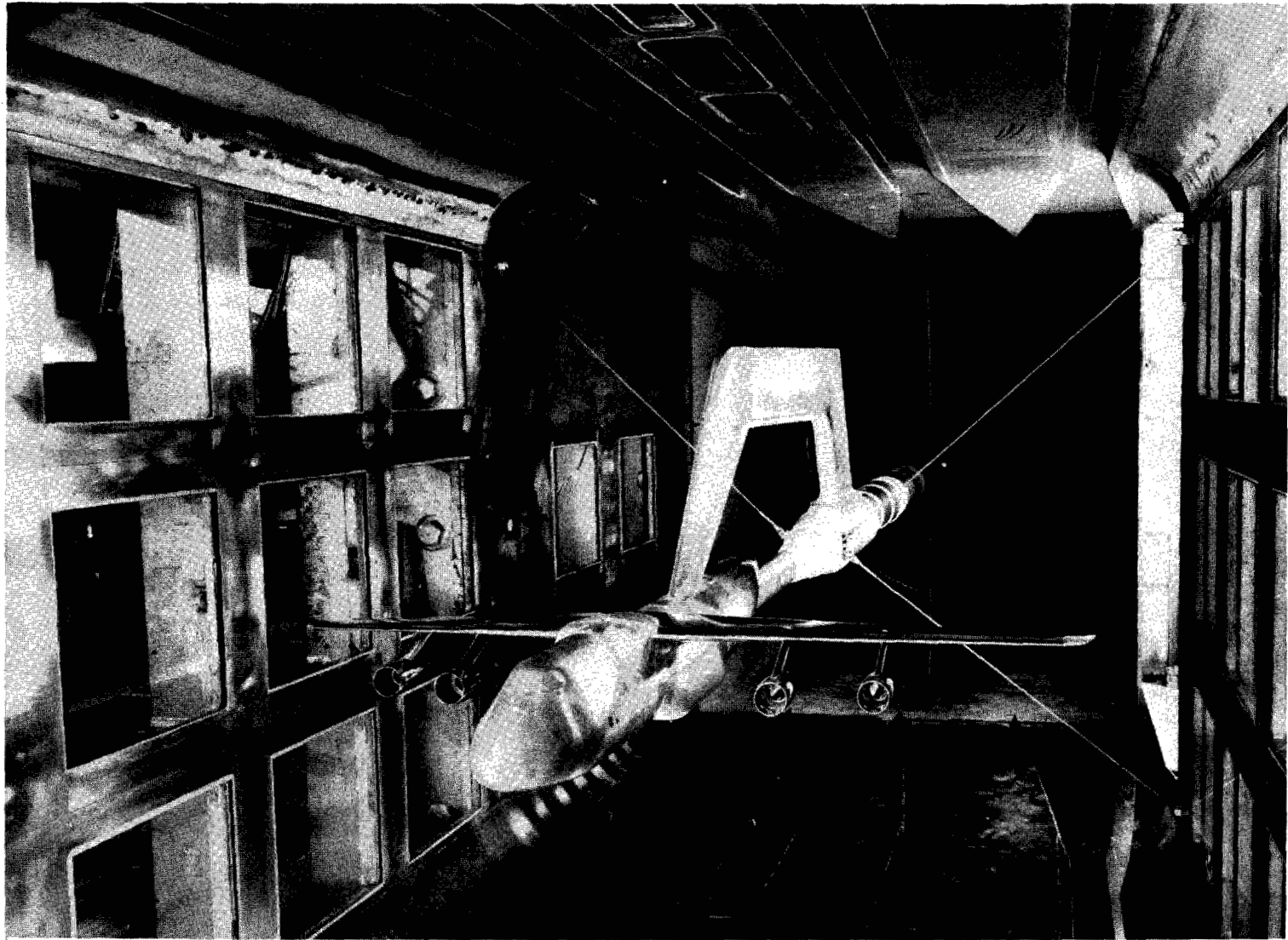


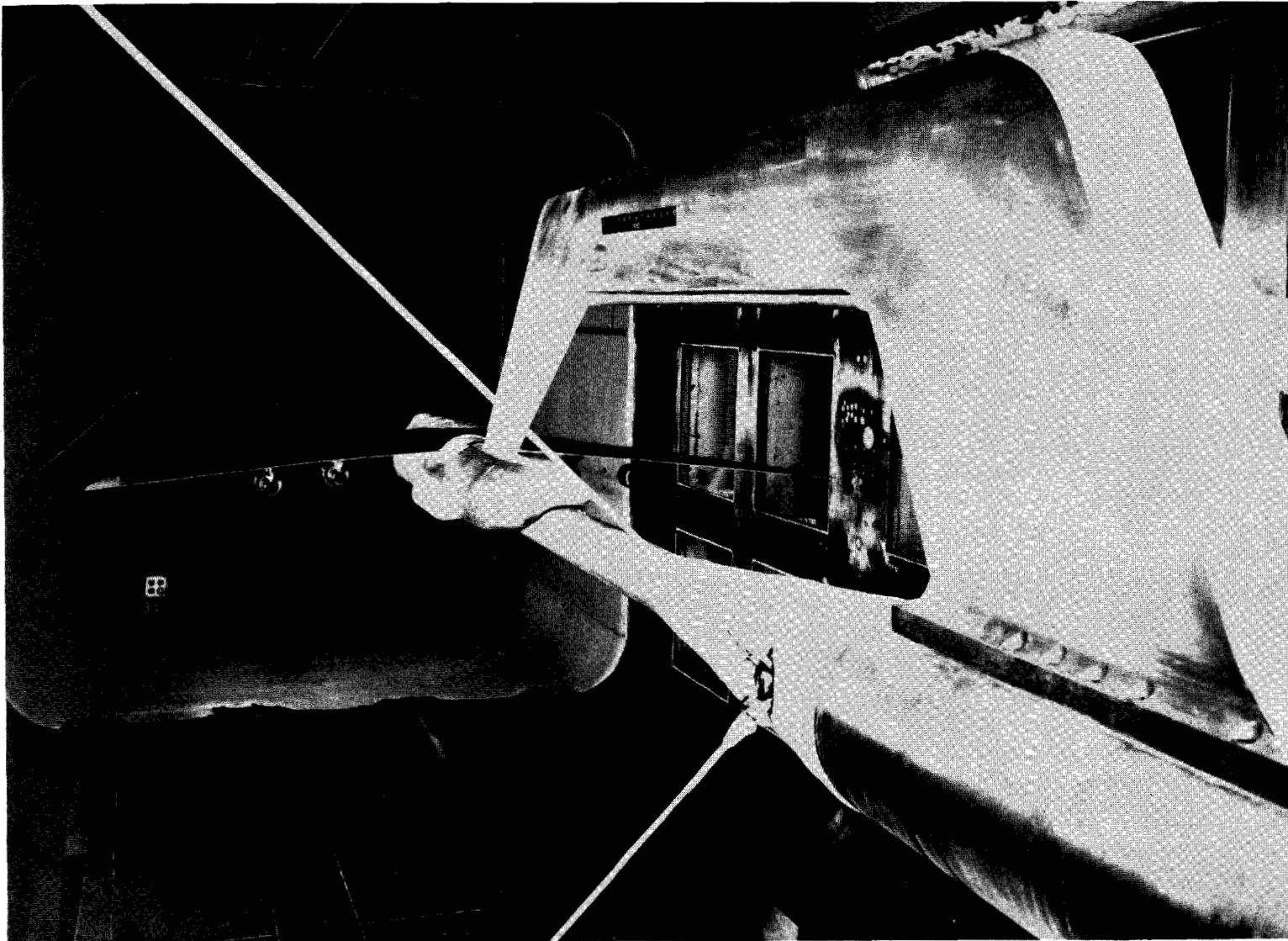
Figure 6.- Details of dorsal strut support with and without dummy sting. All dimensions are in centimeters.



(a) Front quarter view.

L-65-2859

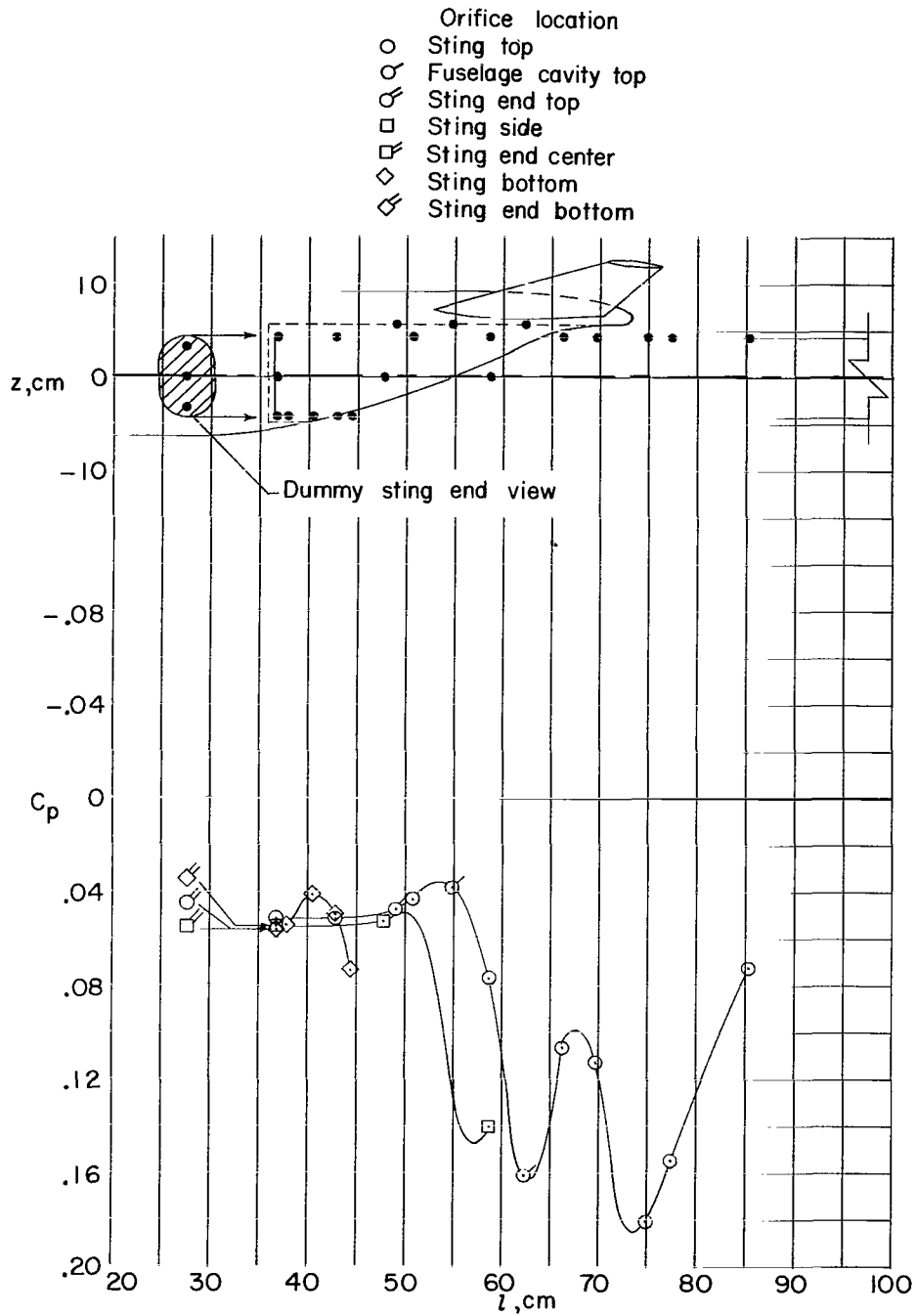
Figure 7.- Photograph of typical cargo-type airplane model supported by dorsal strut with dummy sting present.



(b) Rear quarter view.

L-65-2858

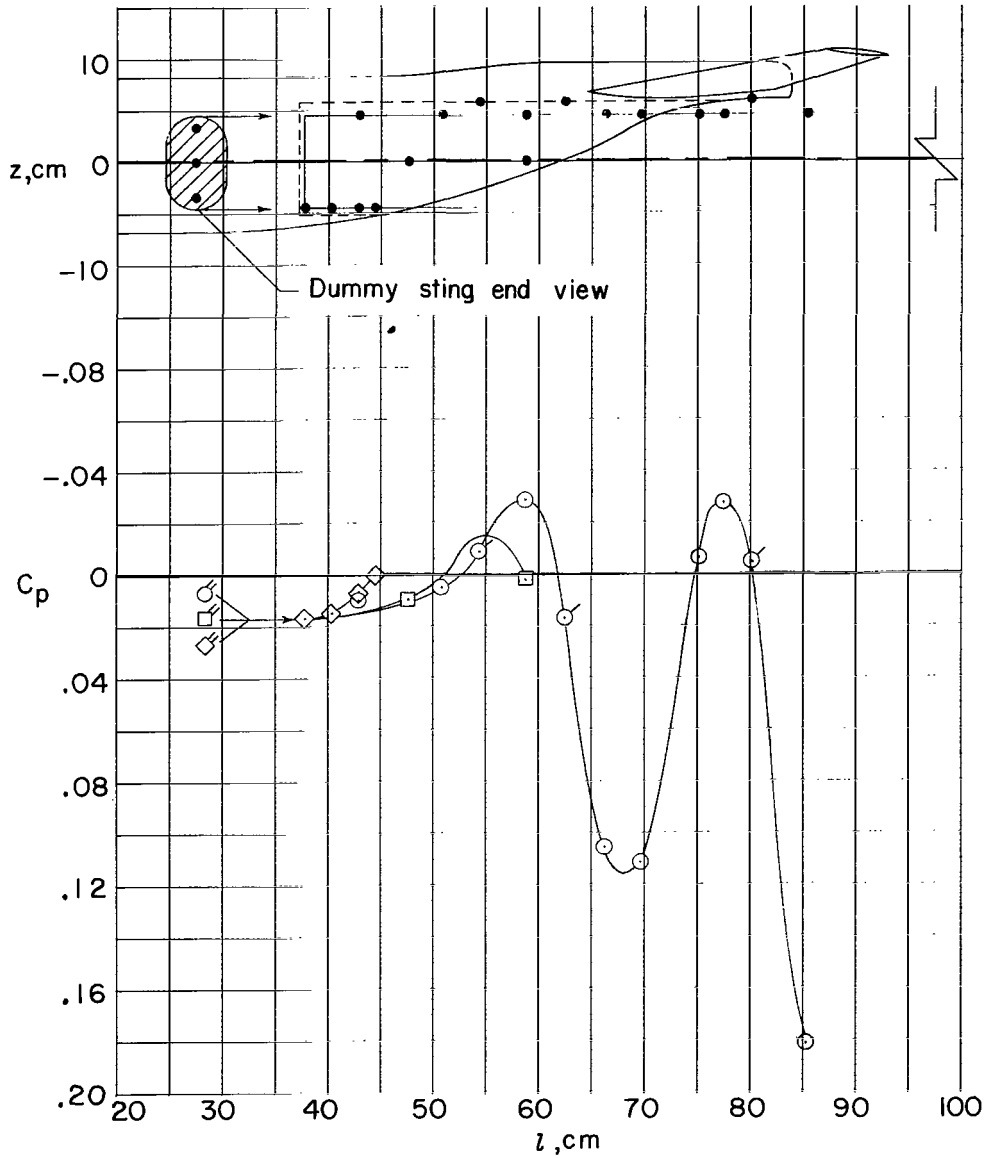
Figure 7.- Concluded.



(a) Model A.

Figure 8.- Longitudinal distribution of pressure coefficients for dummy sting in fuselage cavity. $M = 0.80$; $\alpha = 1^\circ$. Solid dots on sketch indicate orifice locations.

- Orifice location
- Sting top
- Fuselage cavity top
- Sting end top
- Sting side
- Sting end center
- ◇ Sting bottom
- ◇ Sting end bottom



(b) Model B.

Figure 8.- Continued.

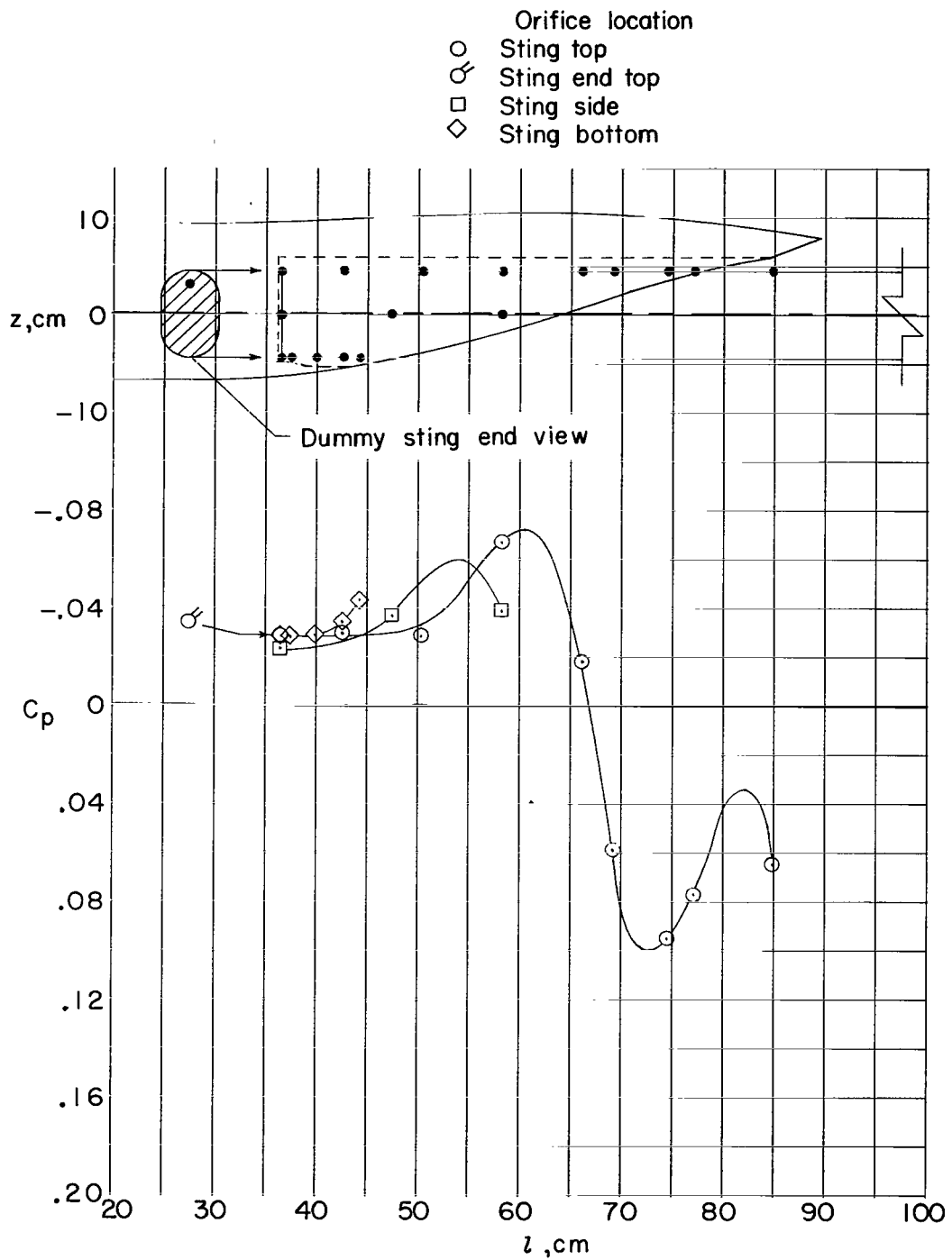


Figure 8.- Concluded.

Type of run

Support system

Each balance measurement includes the following:

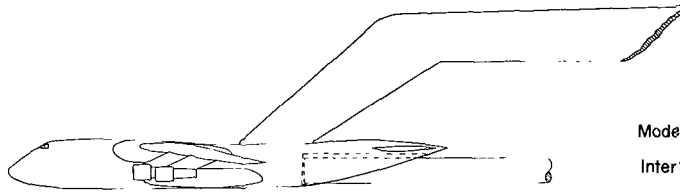
Normal run



Conventional live sting

Model force
Interference of sting on model

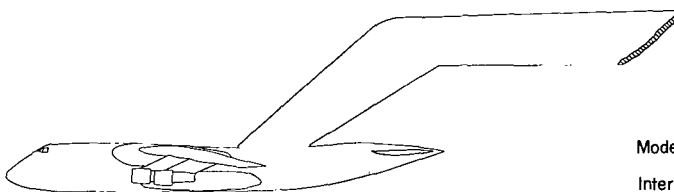
Tare run A



Dorsal strut with dummy sting

Model force
Interference of strut on model
Interference of sting on model

Tare run B



Dorsal strut

Model force
Interference of strut on model

Tare run A - Tare run B = Interference of sting on model
(Sting tare)

Normal run - (Tare run A - Tare run B) = Model force

Figure 9.- Procedure for obtaining sting-support interference.

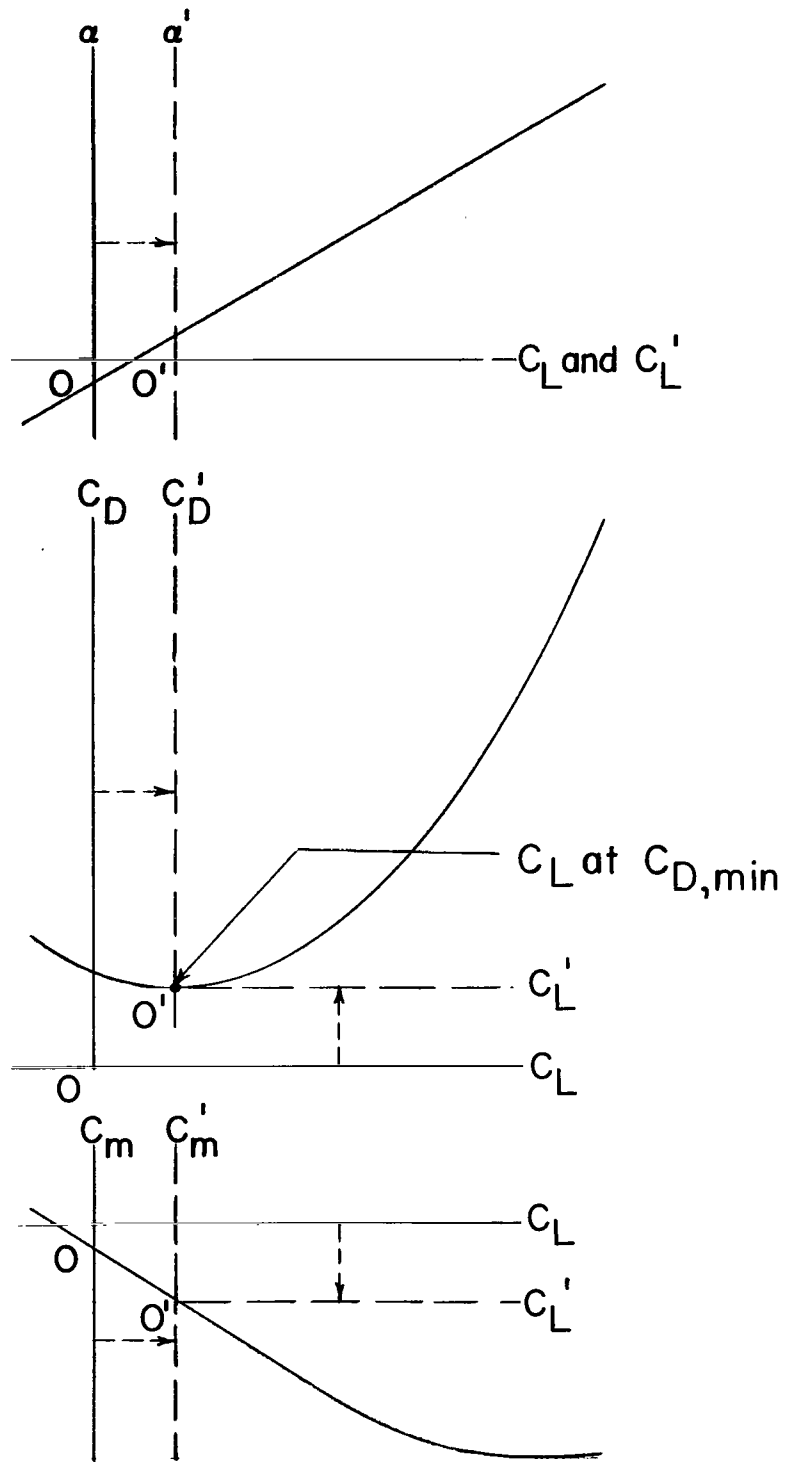
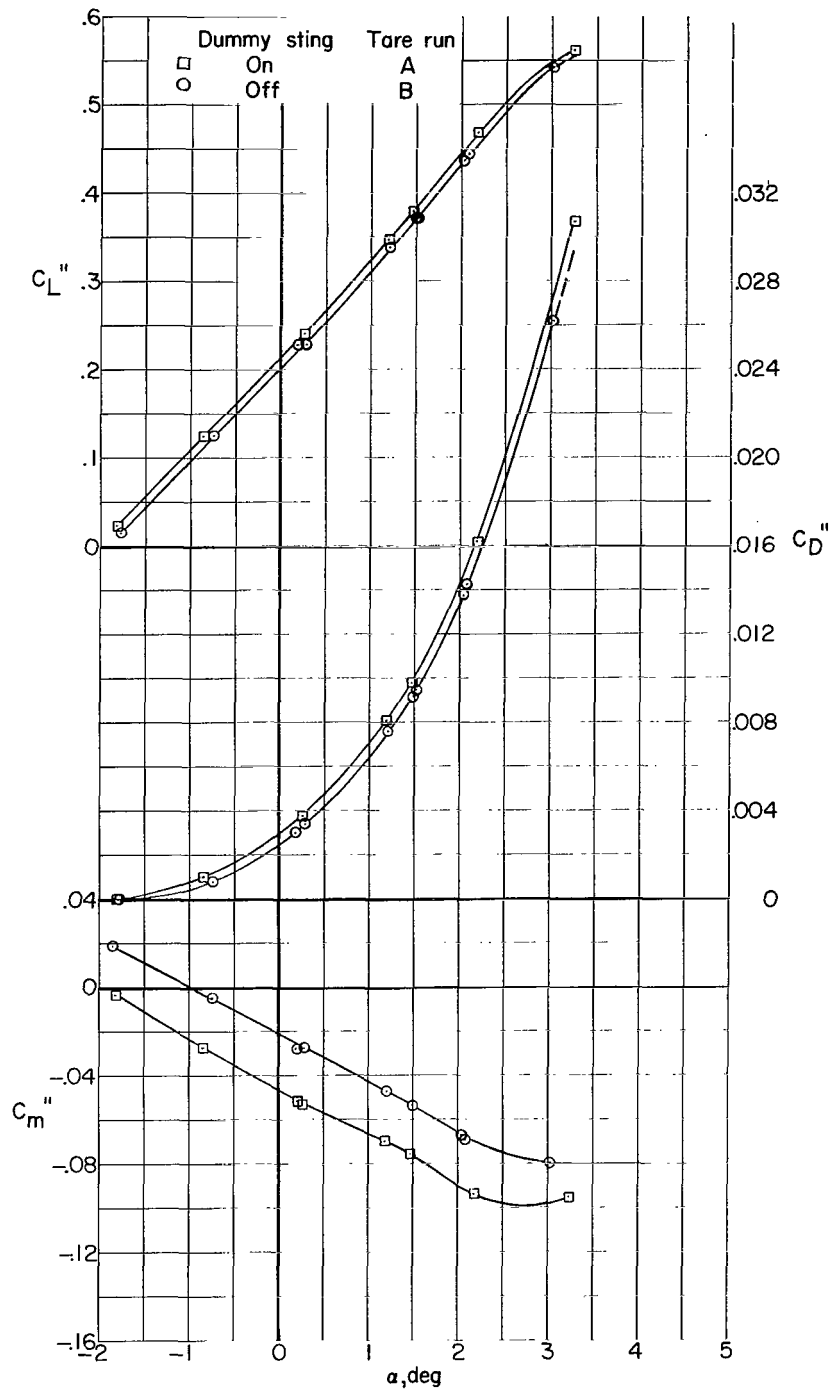
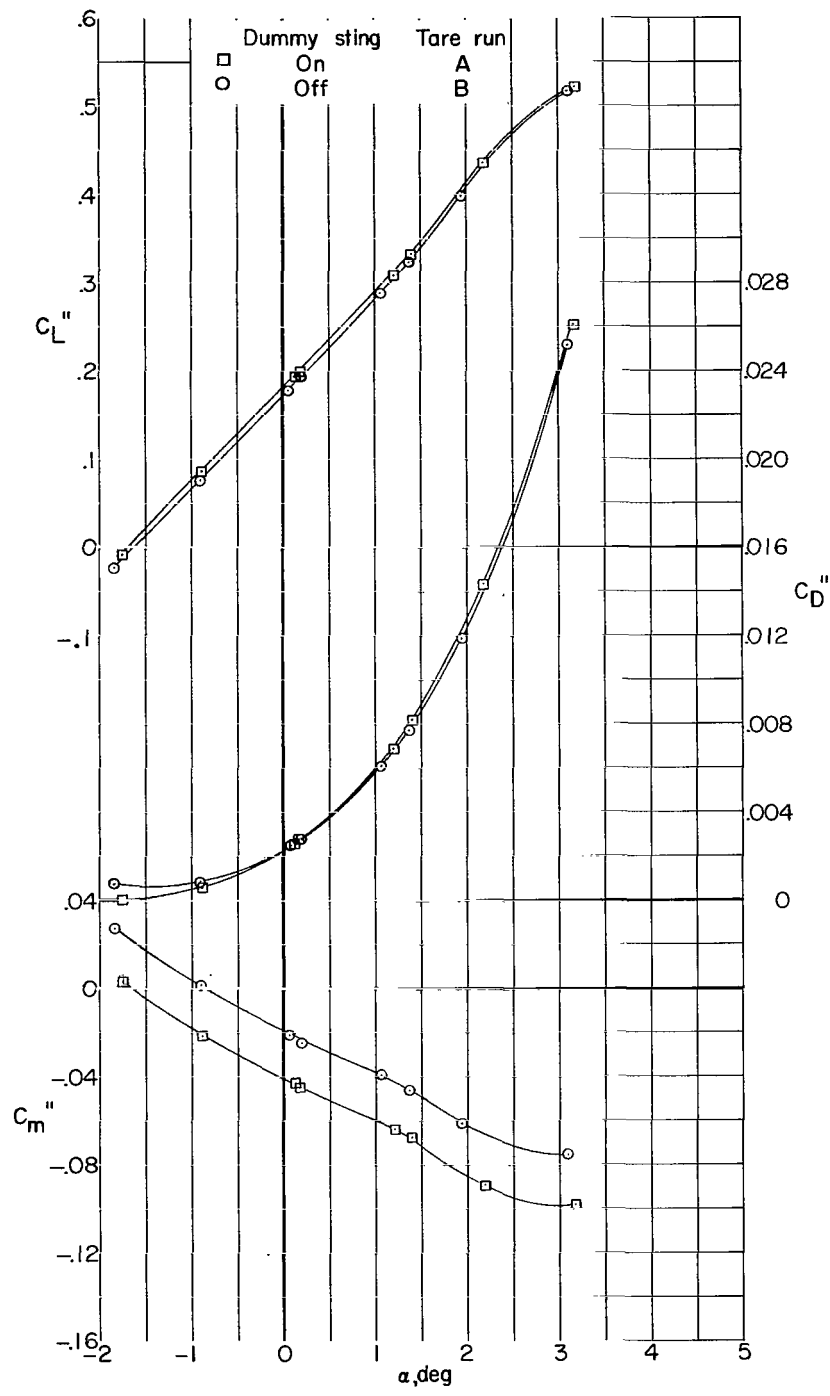


Figure 10.- Method for translating axes to obtain force and moment coefficients in incremental form. $\alpha \equiv \alpha'$.



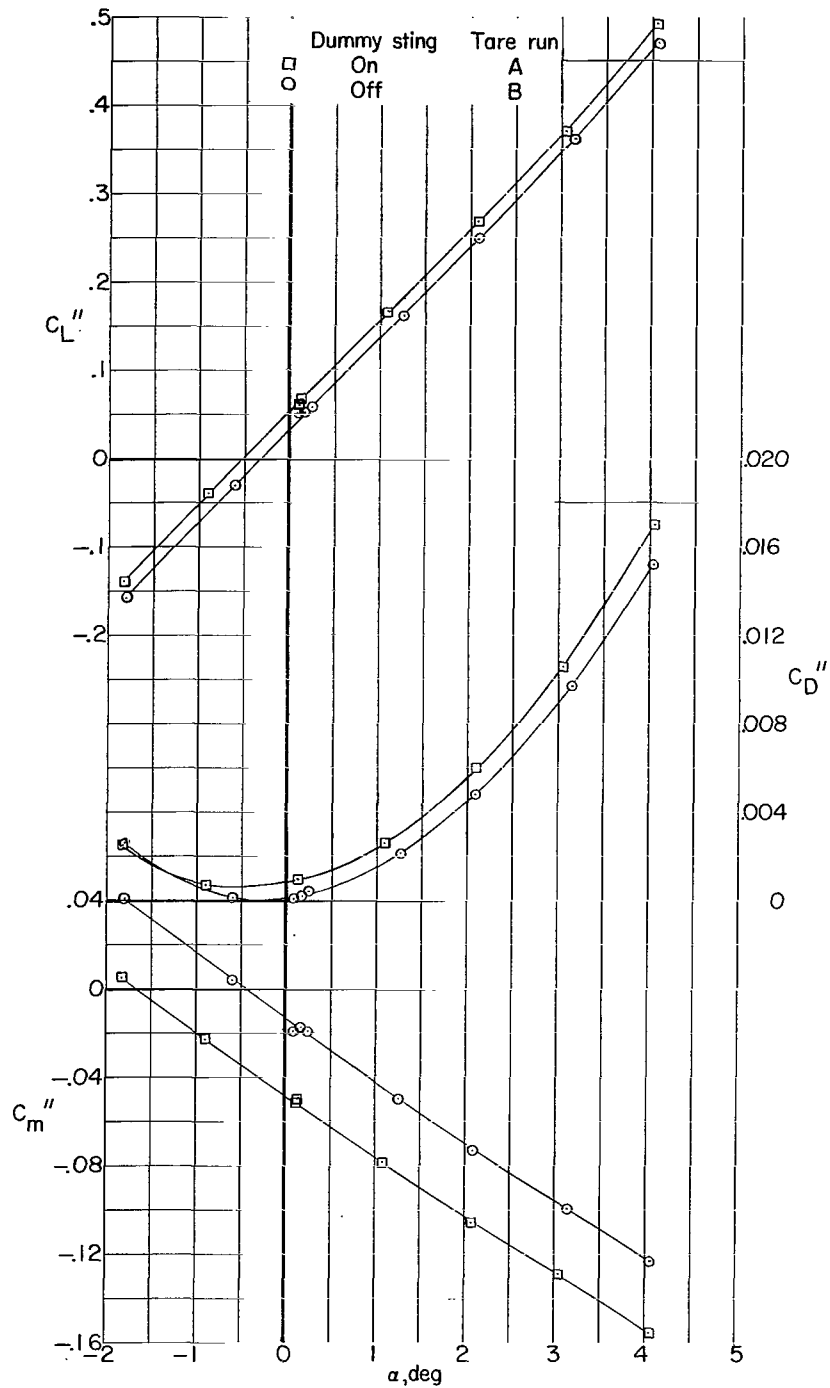
(a) $\delta_h = -0.1^\circ$.

Figure 11.- Variation with angle of attack of lift, drag, and pitching-moment coefficients for model A supported by dorsal strut with and without dummy sting present. $M = 0.80$. Dashed lines indicate extrapolated data.



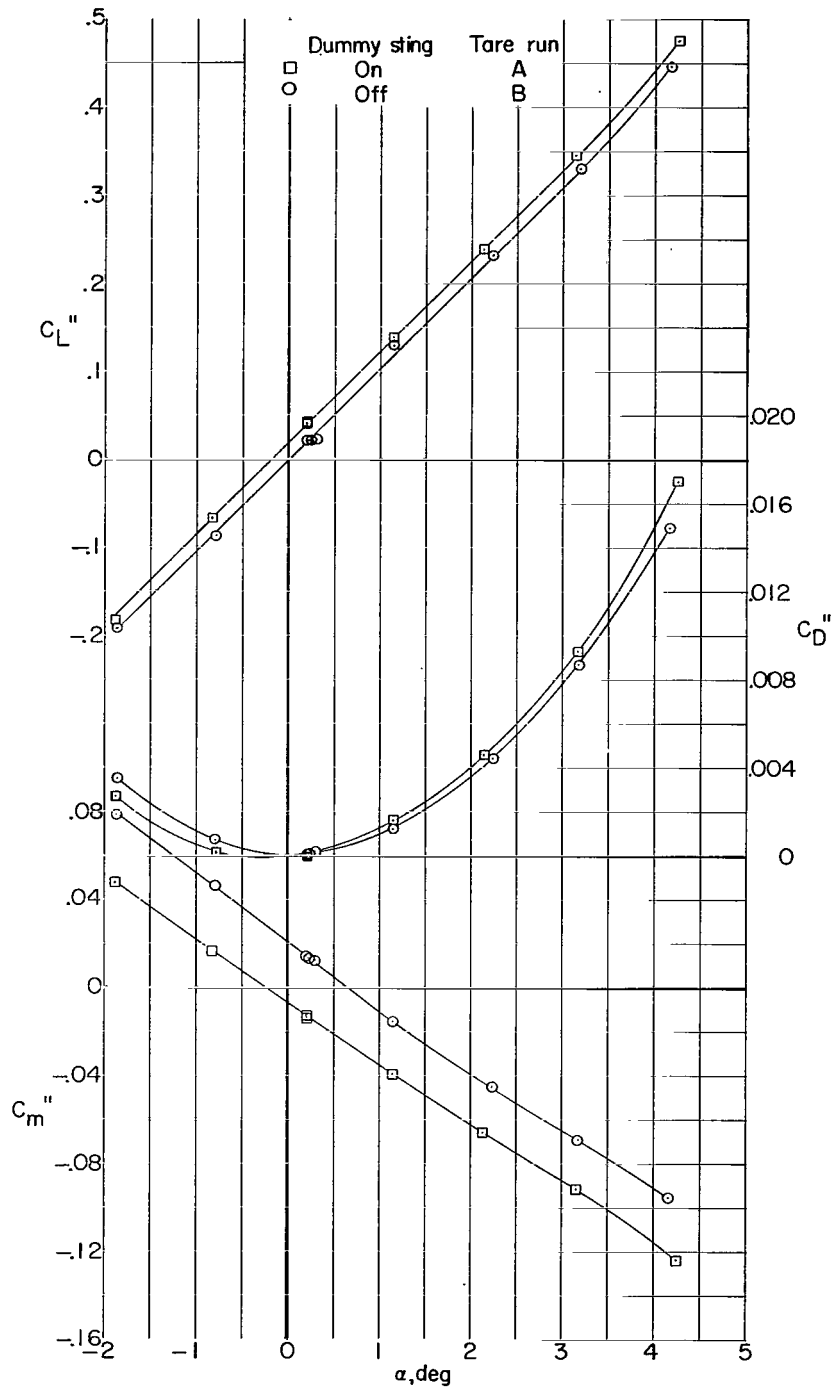
(b) $\delta_h = -1.7^\circ$.

Figure 11.- Concluded.



(a) $\delta_h = 0.2^\circ$.

Figure 12.- Variation with angle of attack of lift, drag, and pitching-moment coefficients for model B supported by dorsal strut with and without dummy sting present. $M \approx 0.80$.



(b) $\delta_h = -1.1^\circ$.

Figure 12.- Concluded.

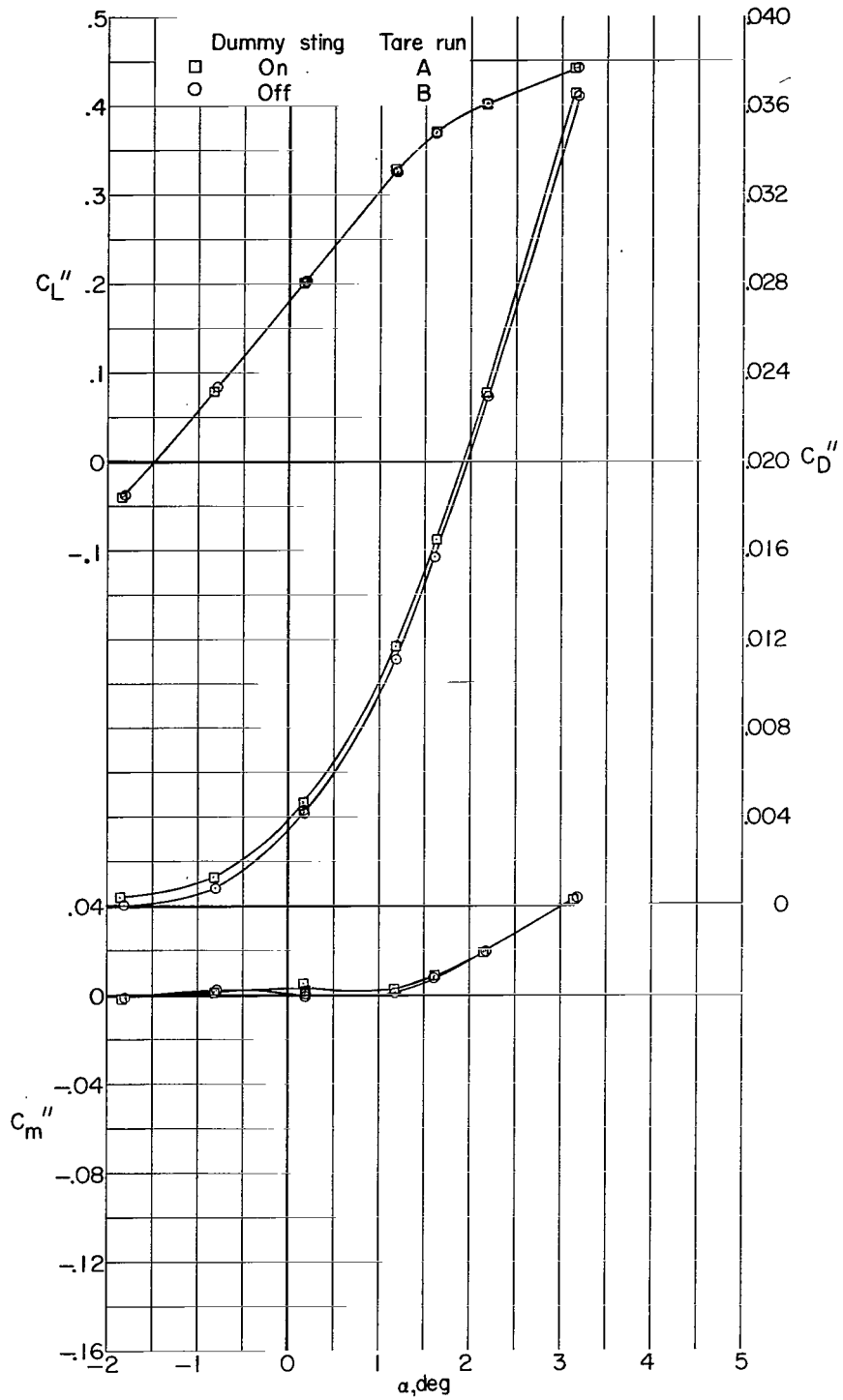
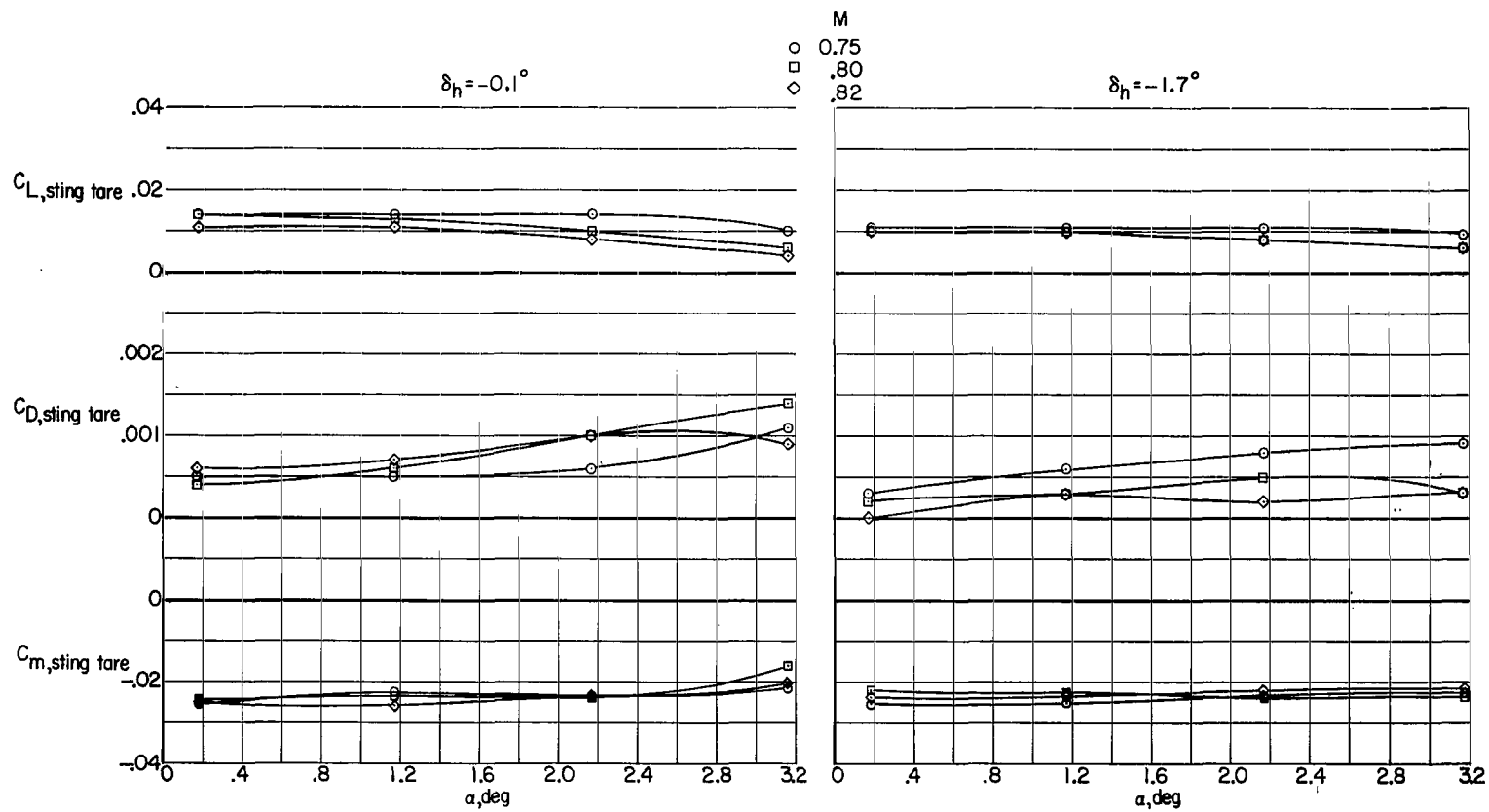
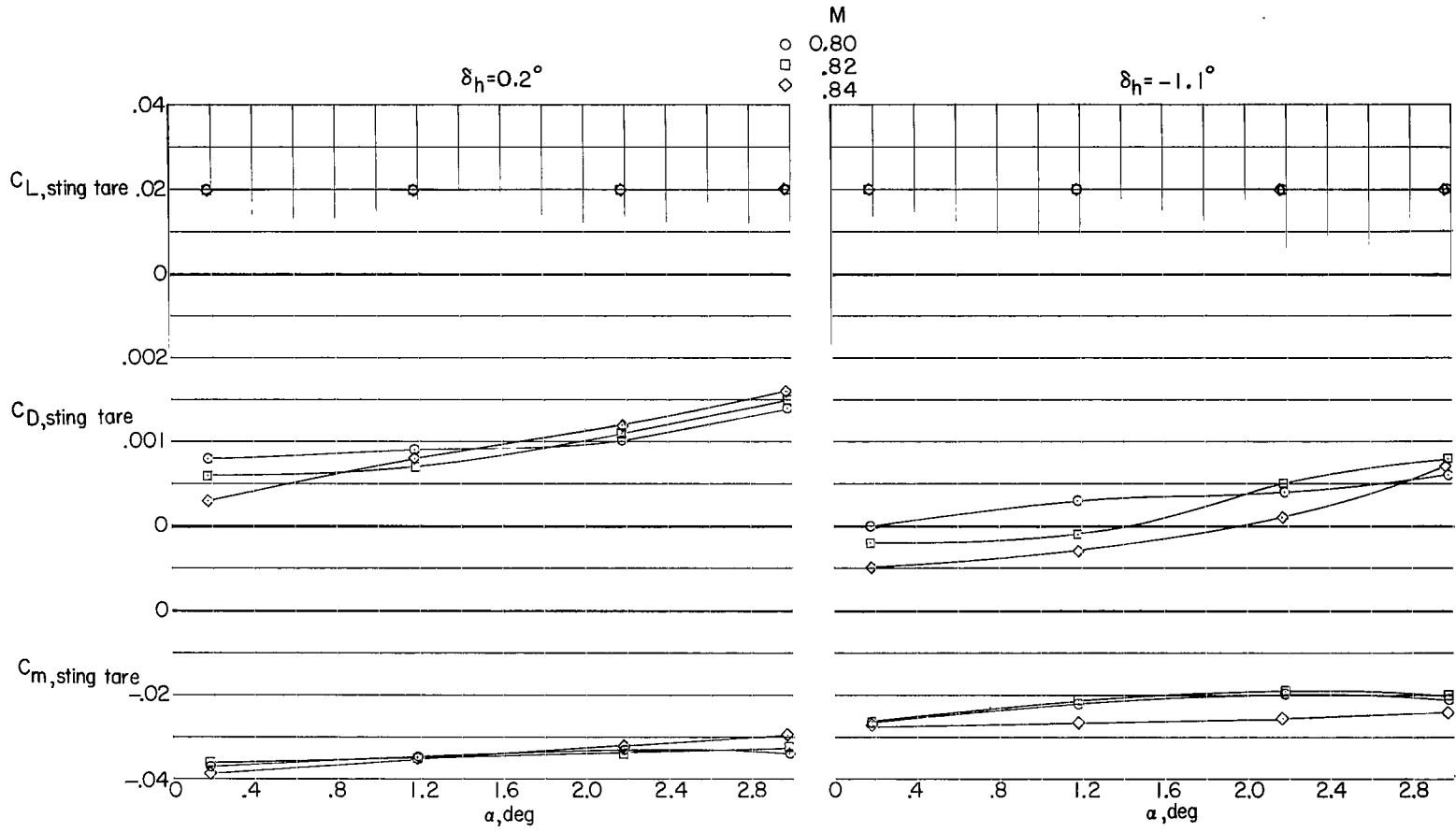


Figure 13.- Variation with angle of attack of lift, drag, and pitching-moment coefficients for model C supported by dorsal strut with and without dummy sting present. $M = 0.80$; horizontal tail off.



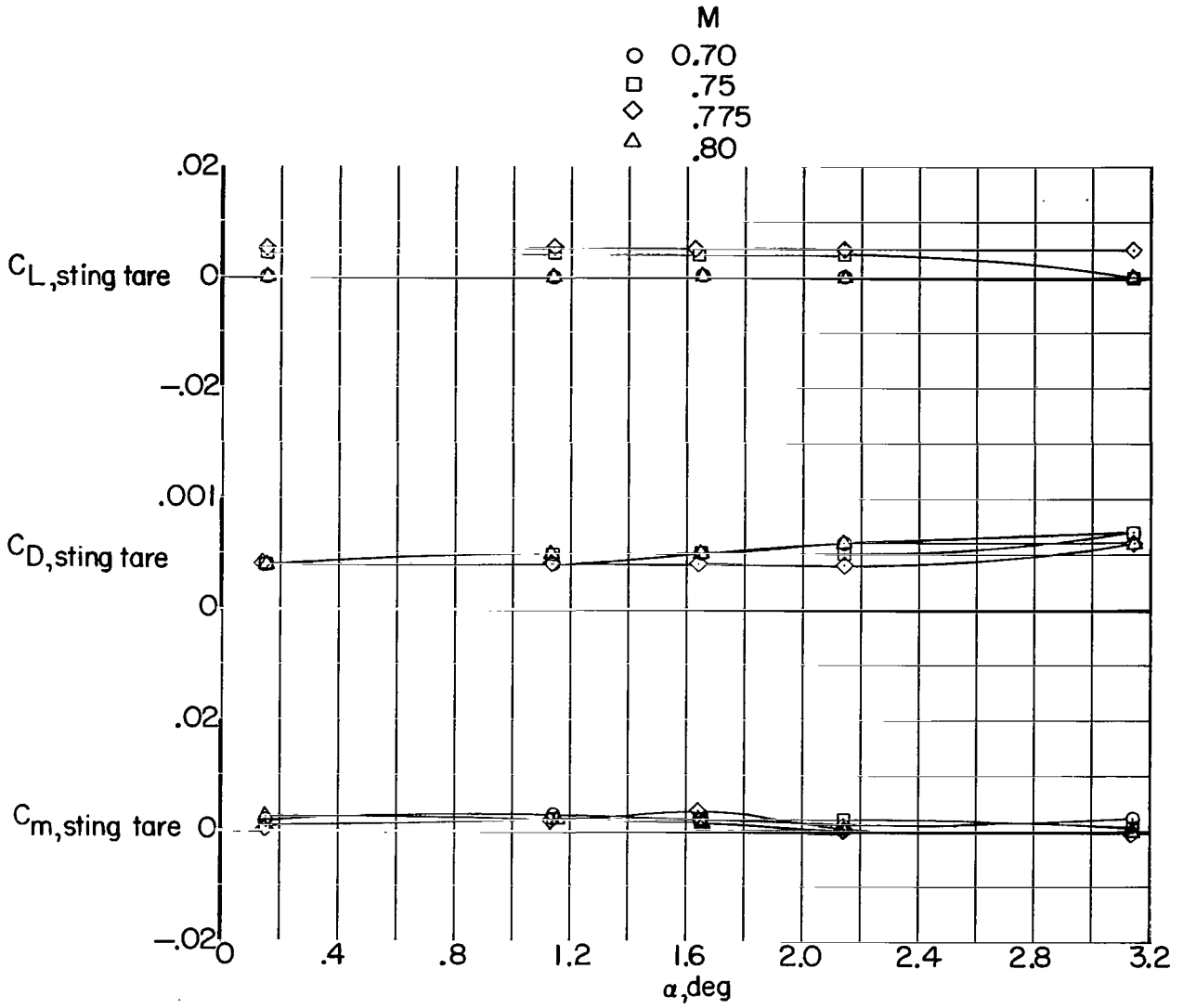
(a) Model A.

Figure 14.- Variation with angle of attack of lift, drag, and pitching-moment sting tares.



(b) Model B.

Figure 14.- Continued.



(c) Model C. Horizontal tail off.

Figure 14.- Concluded.

————— Uncorrected data (Normal run)
 - - - - - Corrected for tares (Model force)

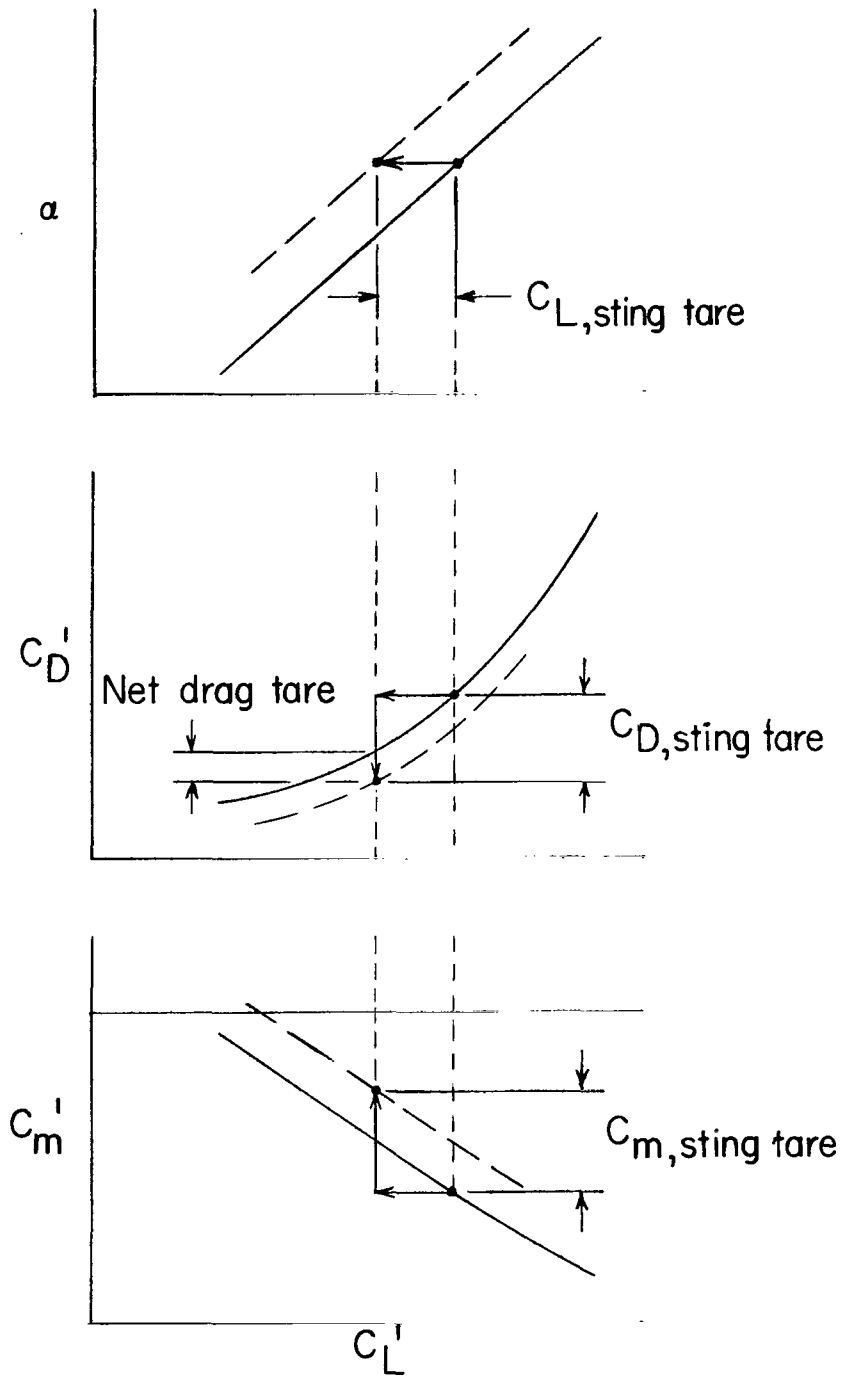
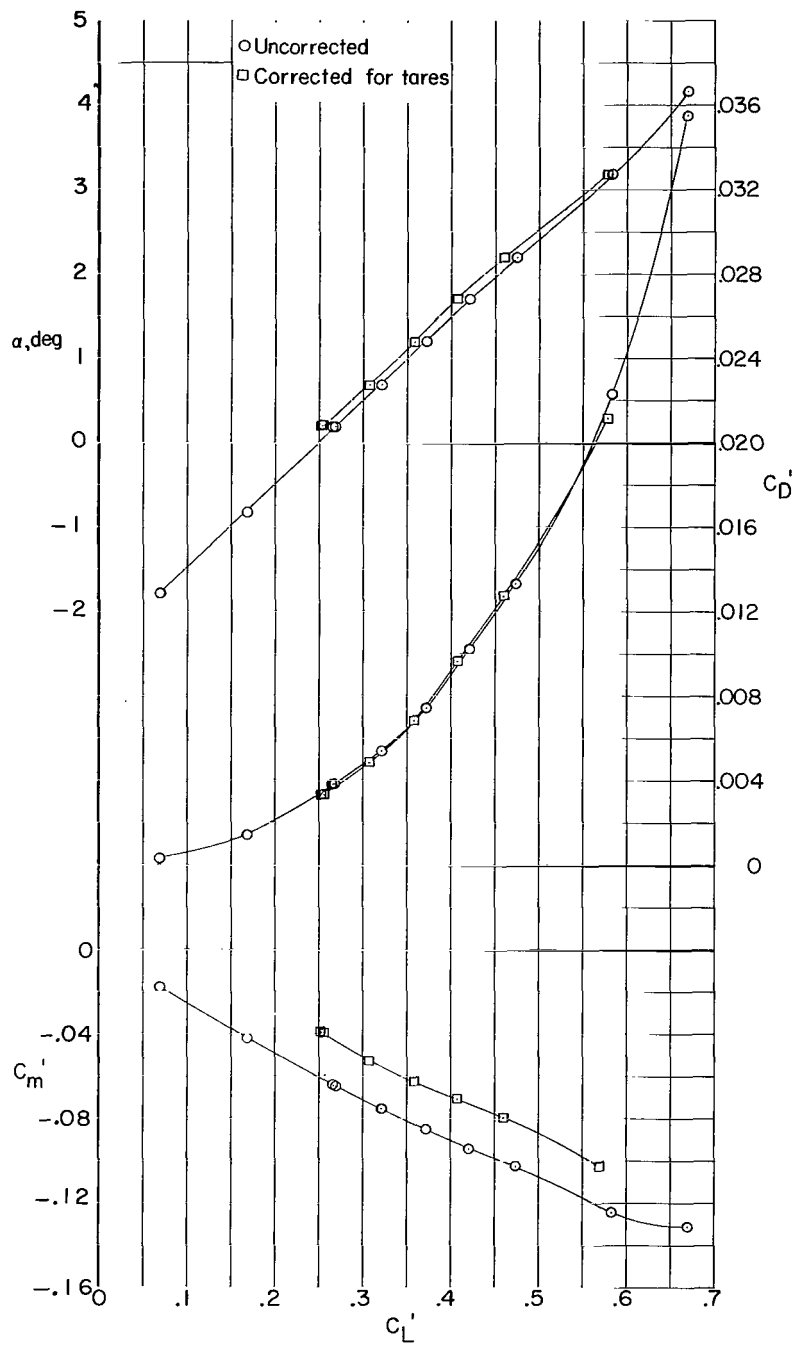
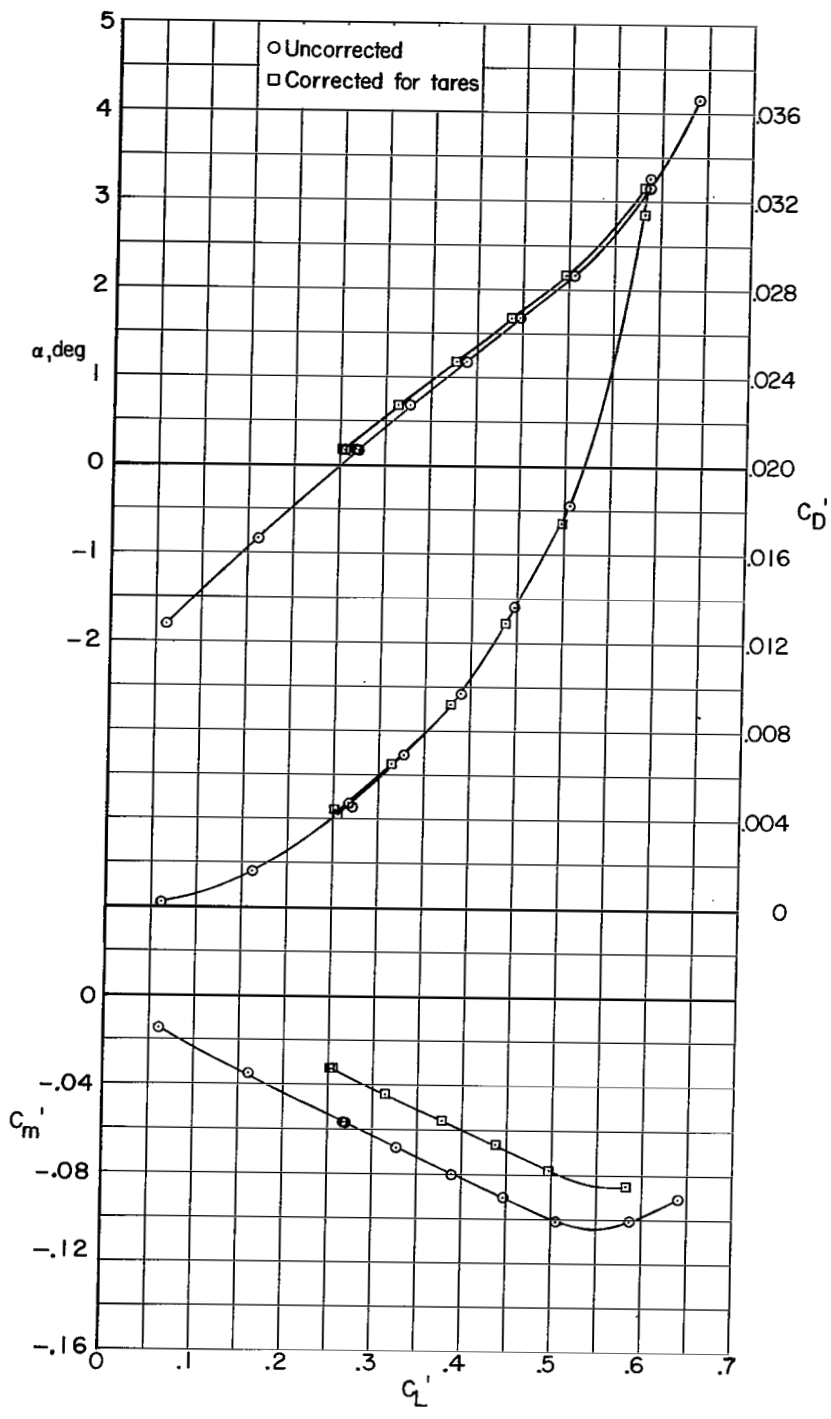


Figure 15.- Method of application of sting tares to uncorrected data and definition of net drag tare.



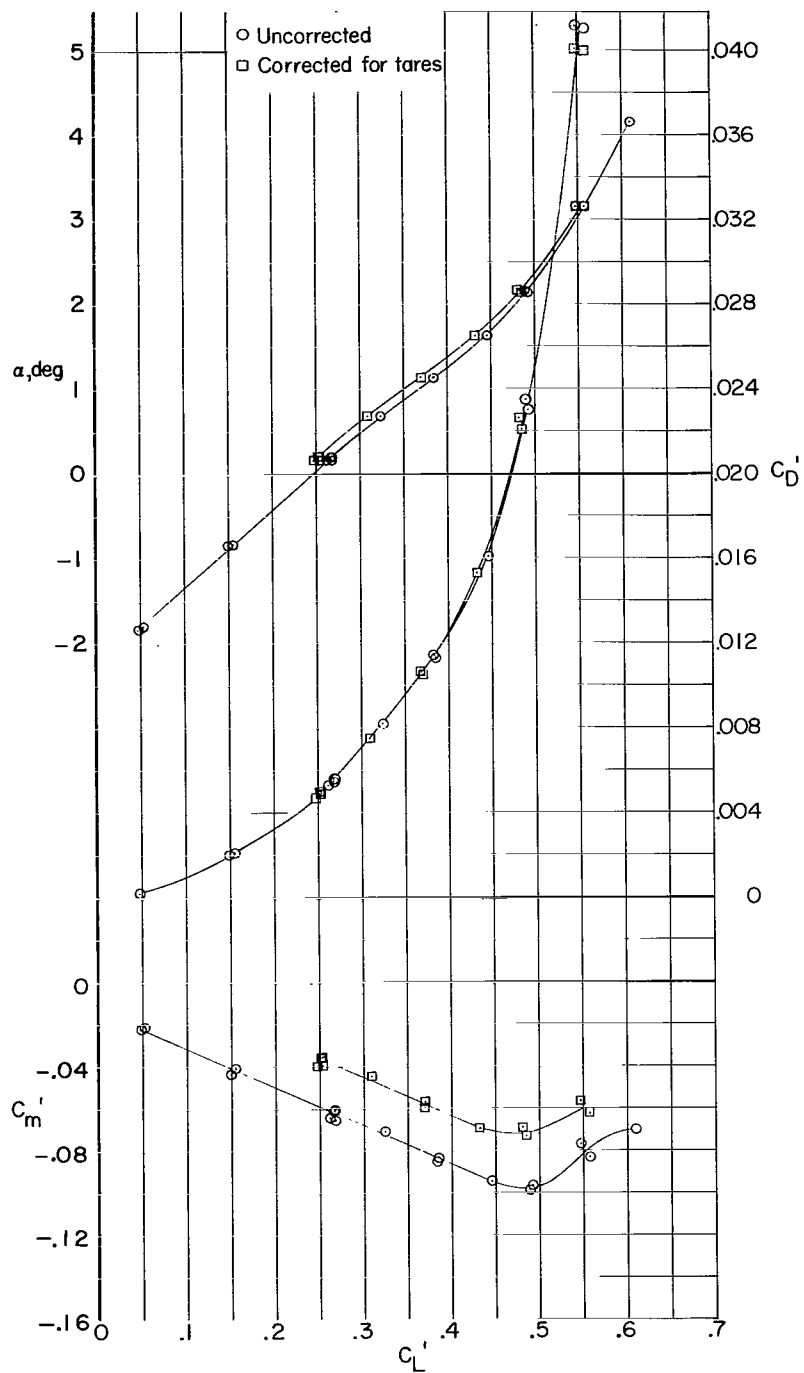
(a) $\delta_h = -0.1^\circ$; $M = 0.75$.

Figure 16.- Variation with lift coefficient of angle of attack, drag, and pitching-moment coefficients uncorrected and corrected for sting tares. Model A.



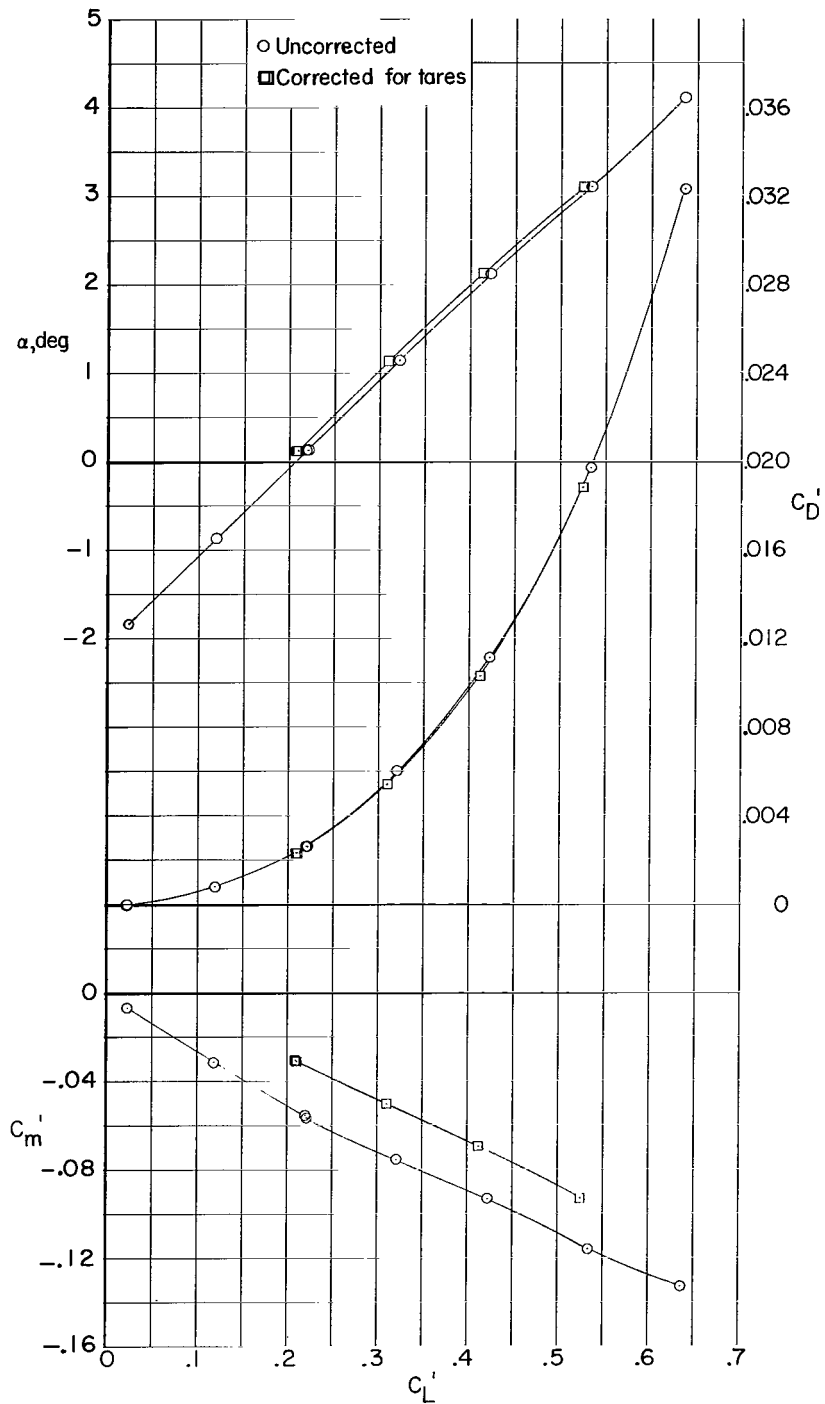
(b) $\delta_h = -0.1^\circ$; $M = 0.80$.

Figure 16.- Continued.



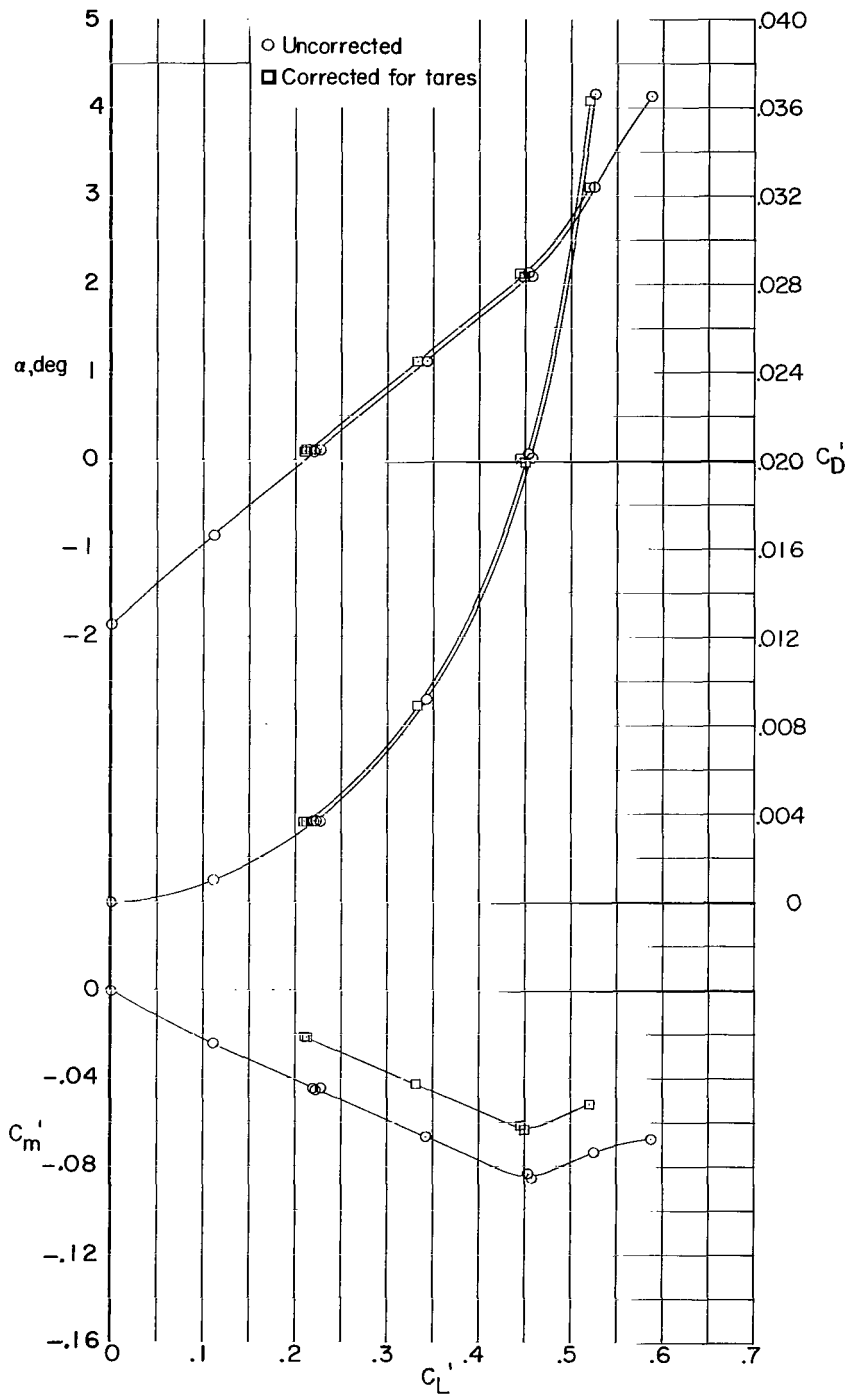
(c) $\delta_h = -0.1^\circ$; $M = 0.82$.

Figure 16.- Continued.



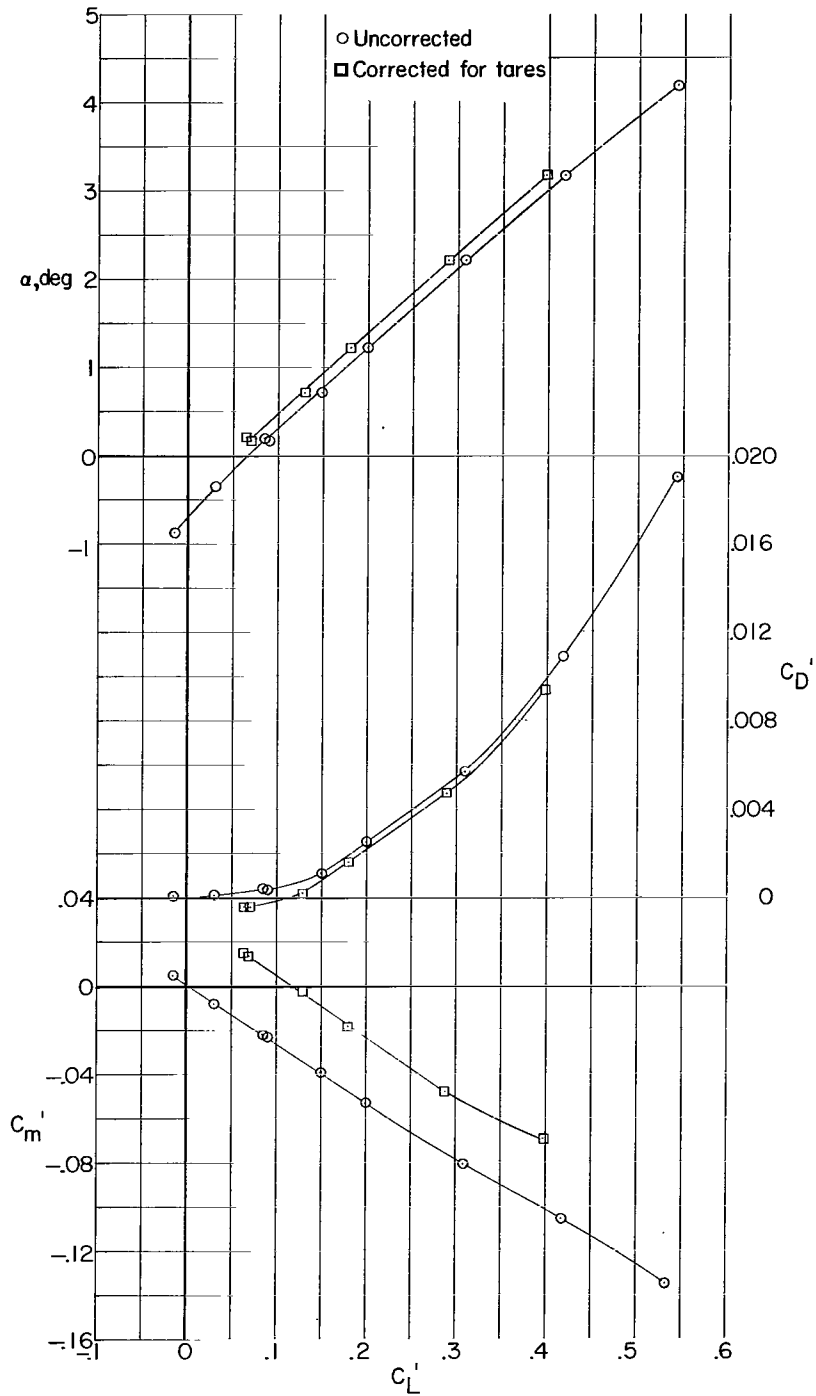
(d) $\delta_h = -1.7^\circ$; $M = 0.75$.

Figure 16.- Continued.



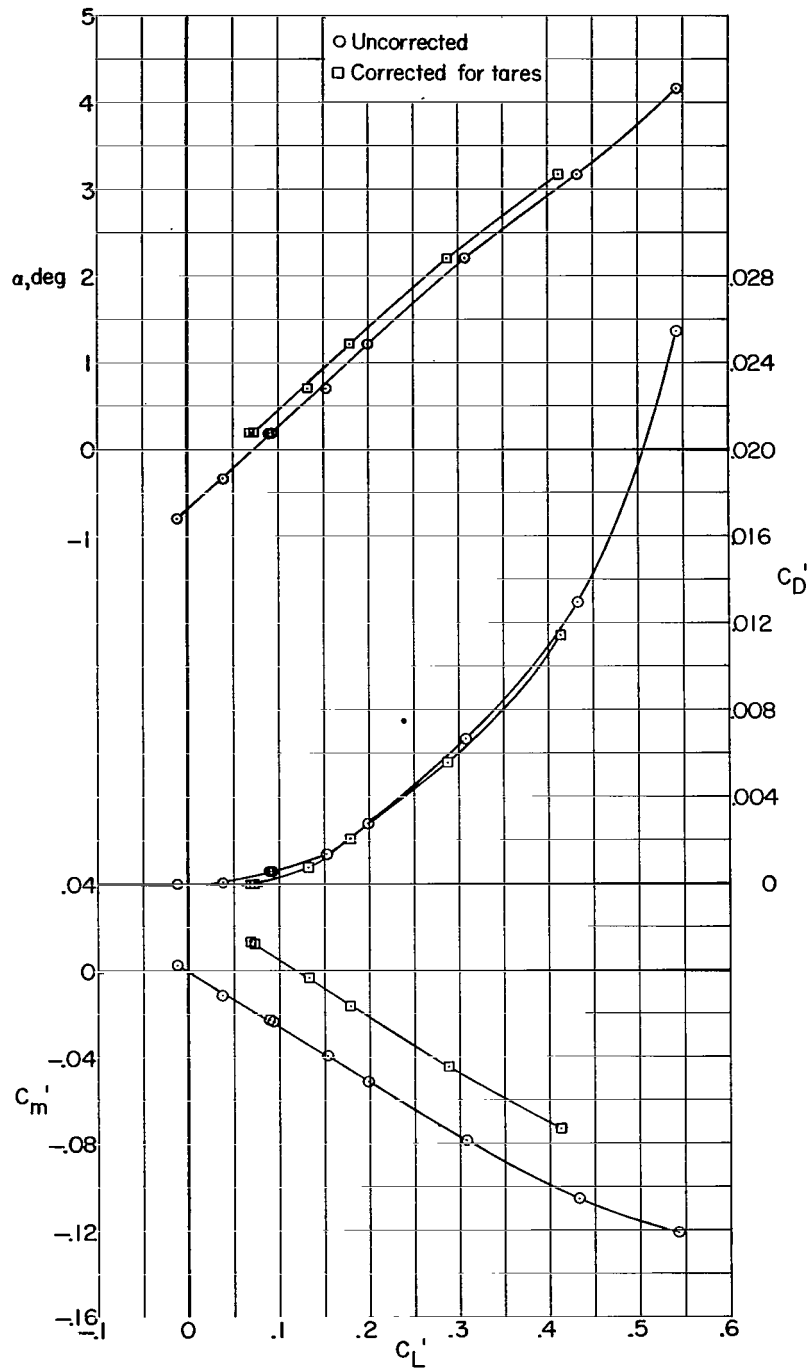
(e) $\delta_h = -1.7^\circ$; $M = 0.82$.

Figure 16.- Concluded.



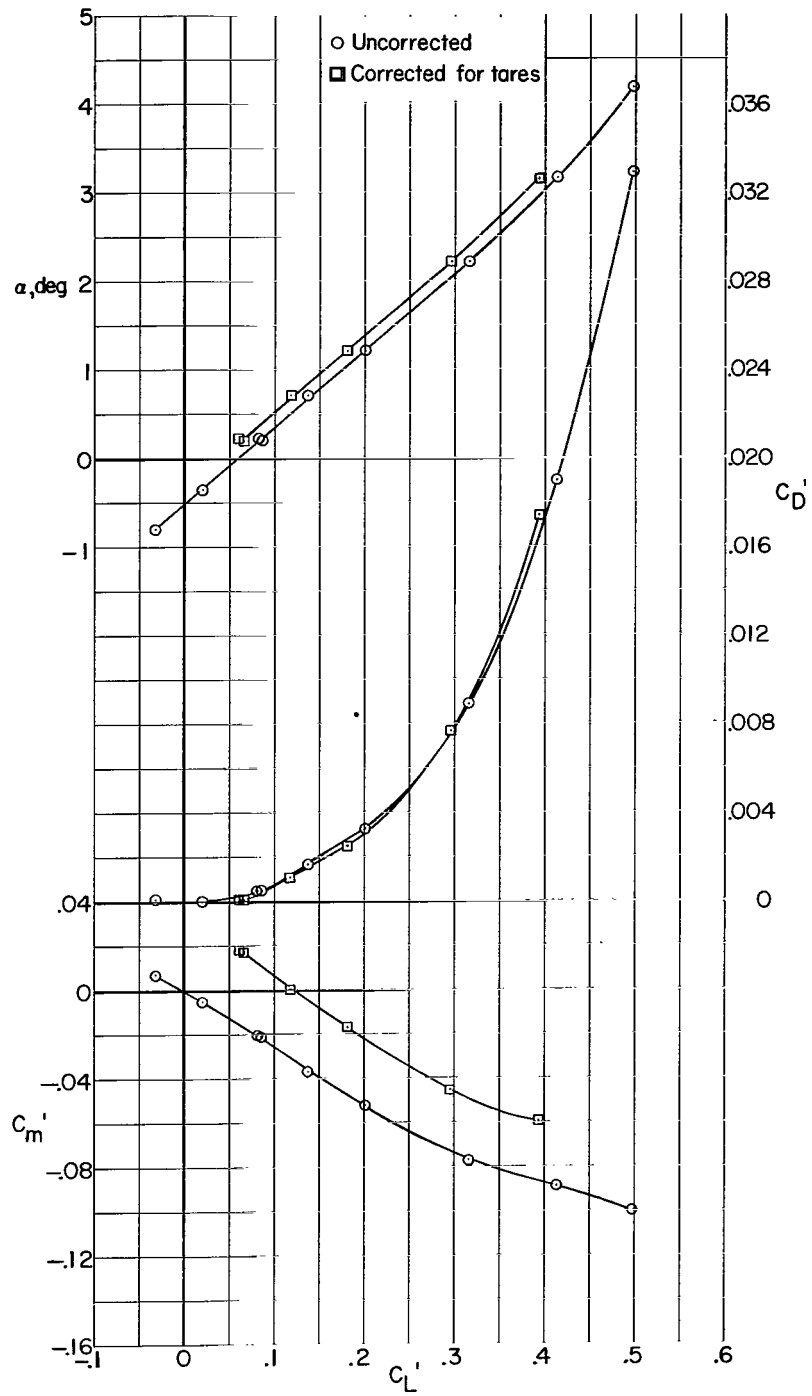
(a) $\delta_h = 0.2^\circ$; $M = 0.80$.

Figure 17.- Variation with lift coefficient of angle of attack, drag, and pitching-moment coefficients uncorrected and corrected for sting tares. Model B.



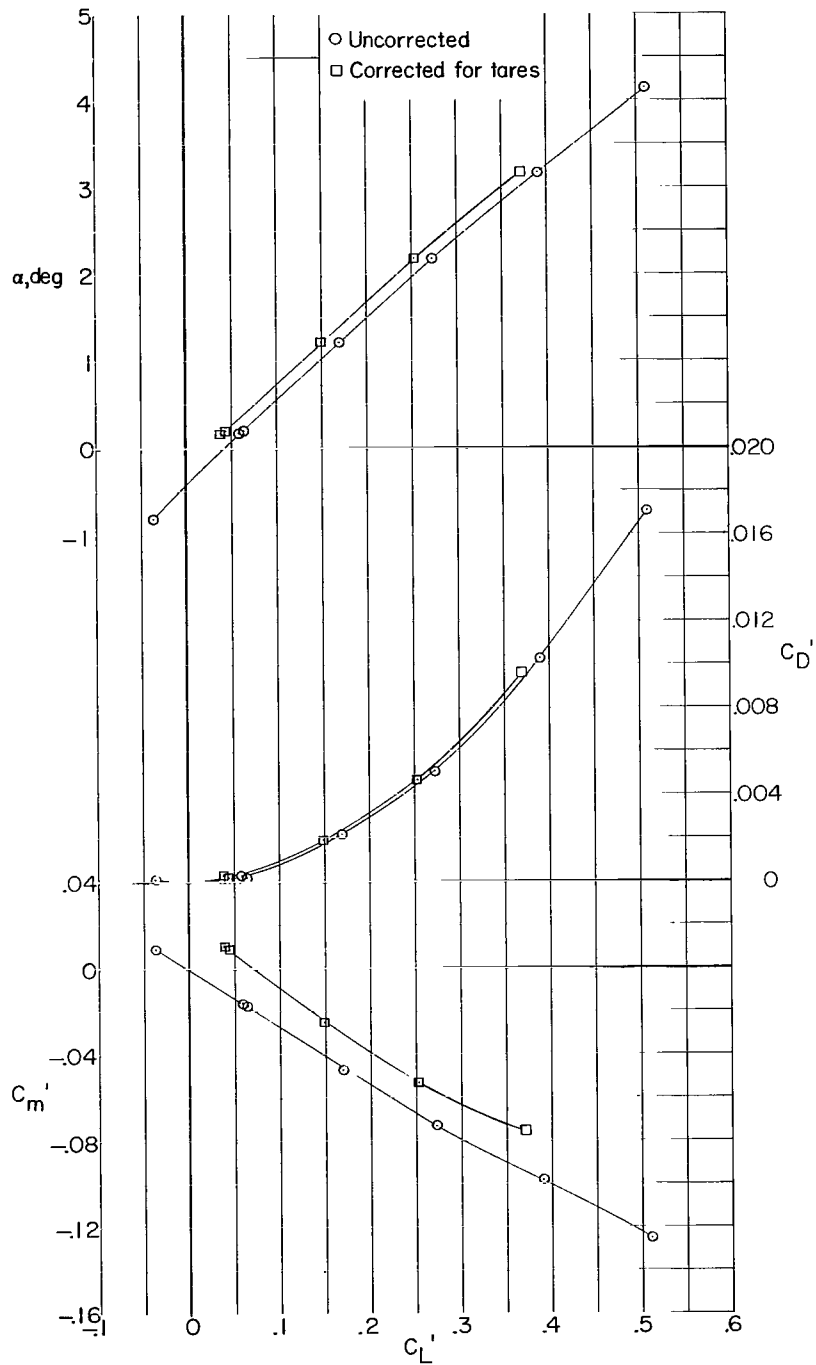
(b) $\delta_h = 0.2^\circ$; $M = 0.82$.

Figure 17.- Continued.



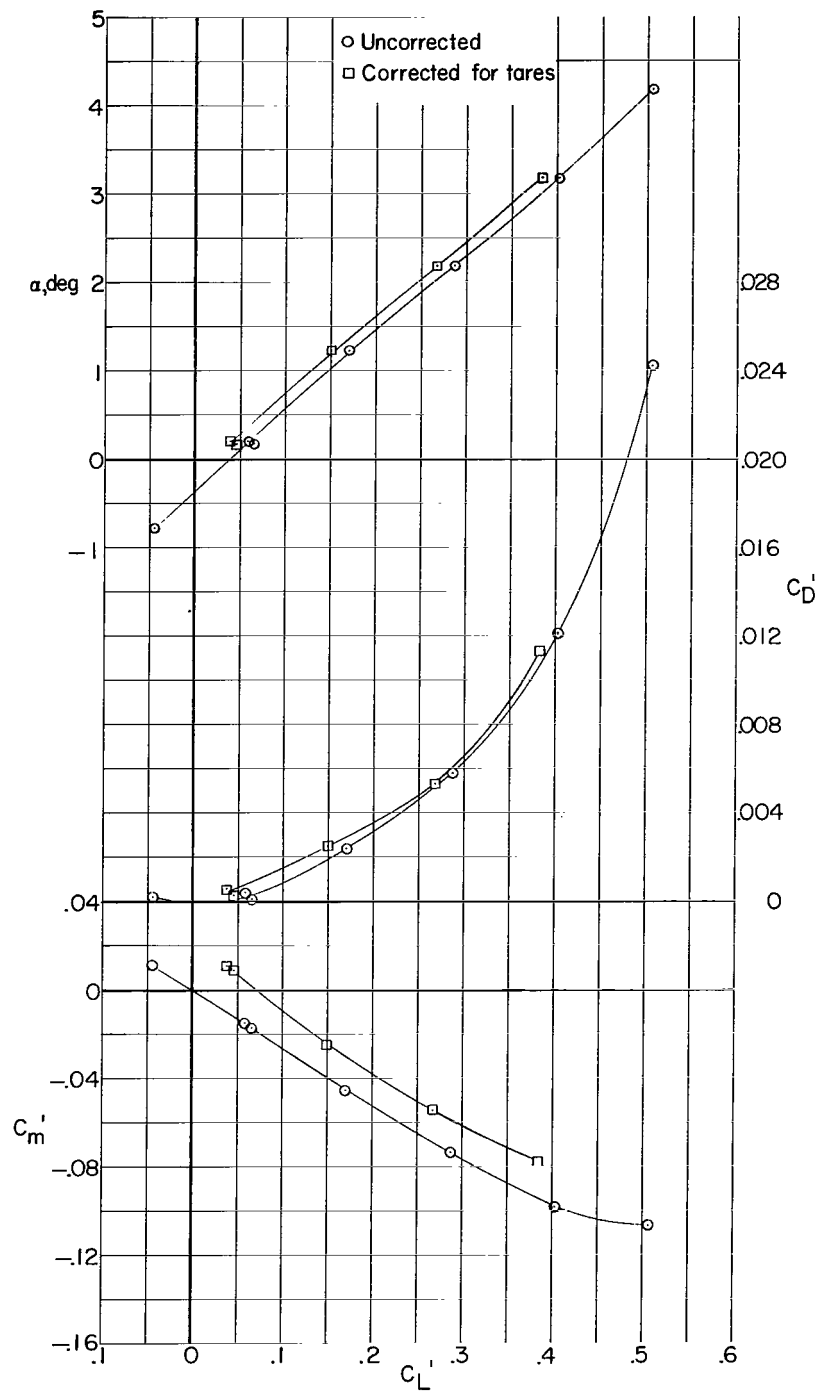
(c) $\delta_h = 0.20$; $M = 0.84$.

Figure 17.- Continued.



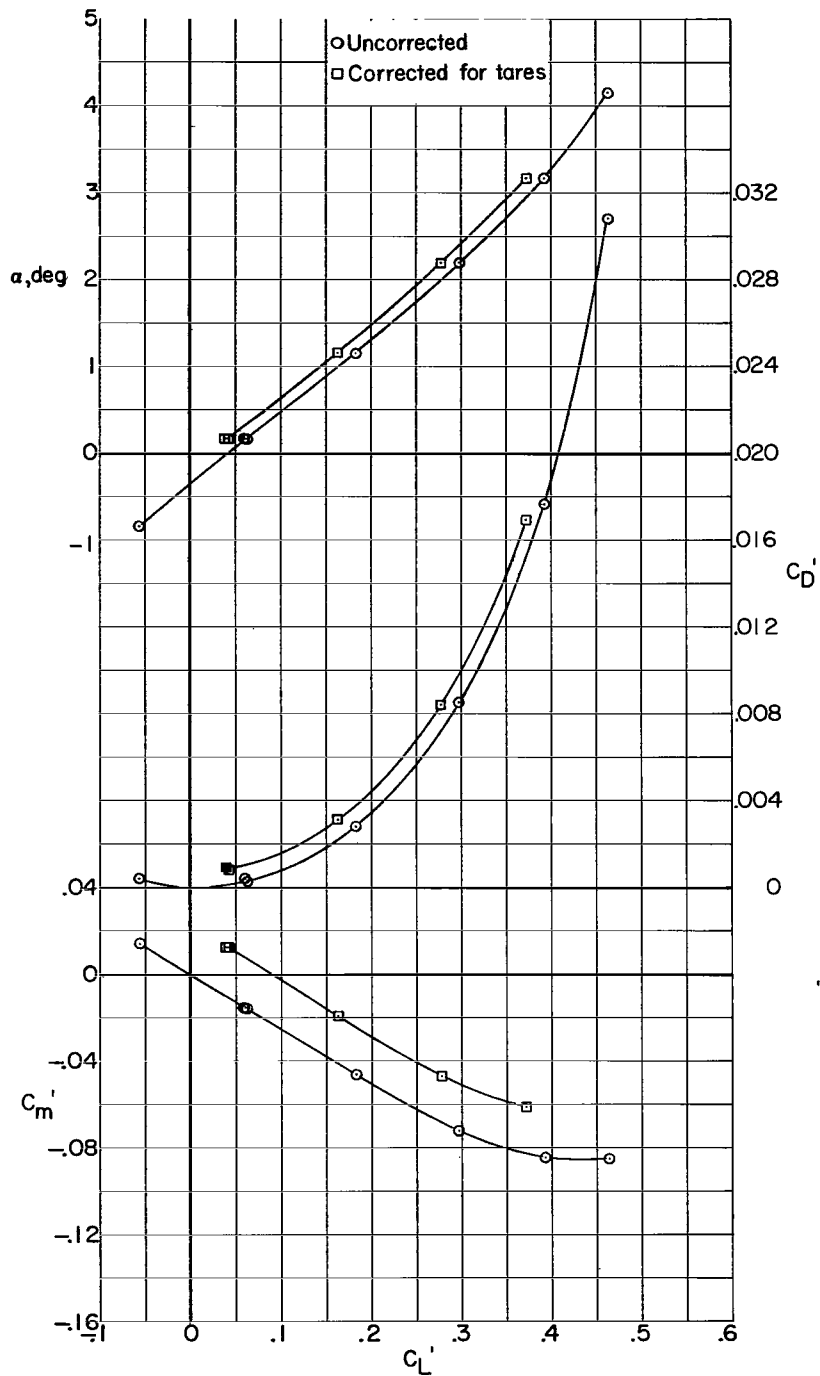
(d) $\delta_h = -1.1^\circ$; $M = 0.80$.

Figure 17.- Continued.



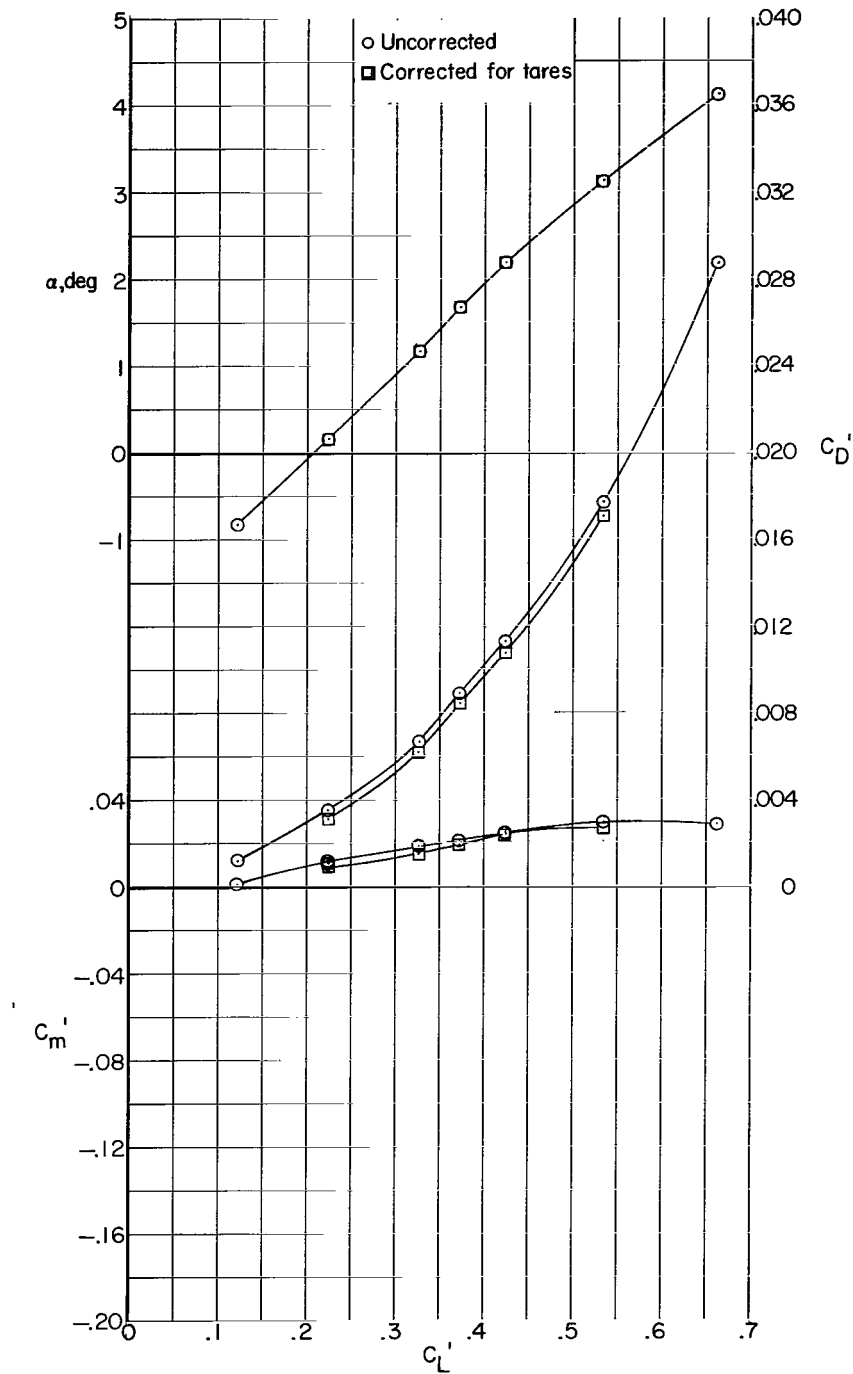
(e) $\delta_h = -1.1^\circ$; $M = 0.82$.

Figure 17.- Continued.



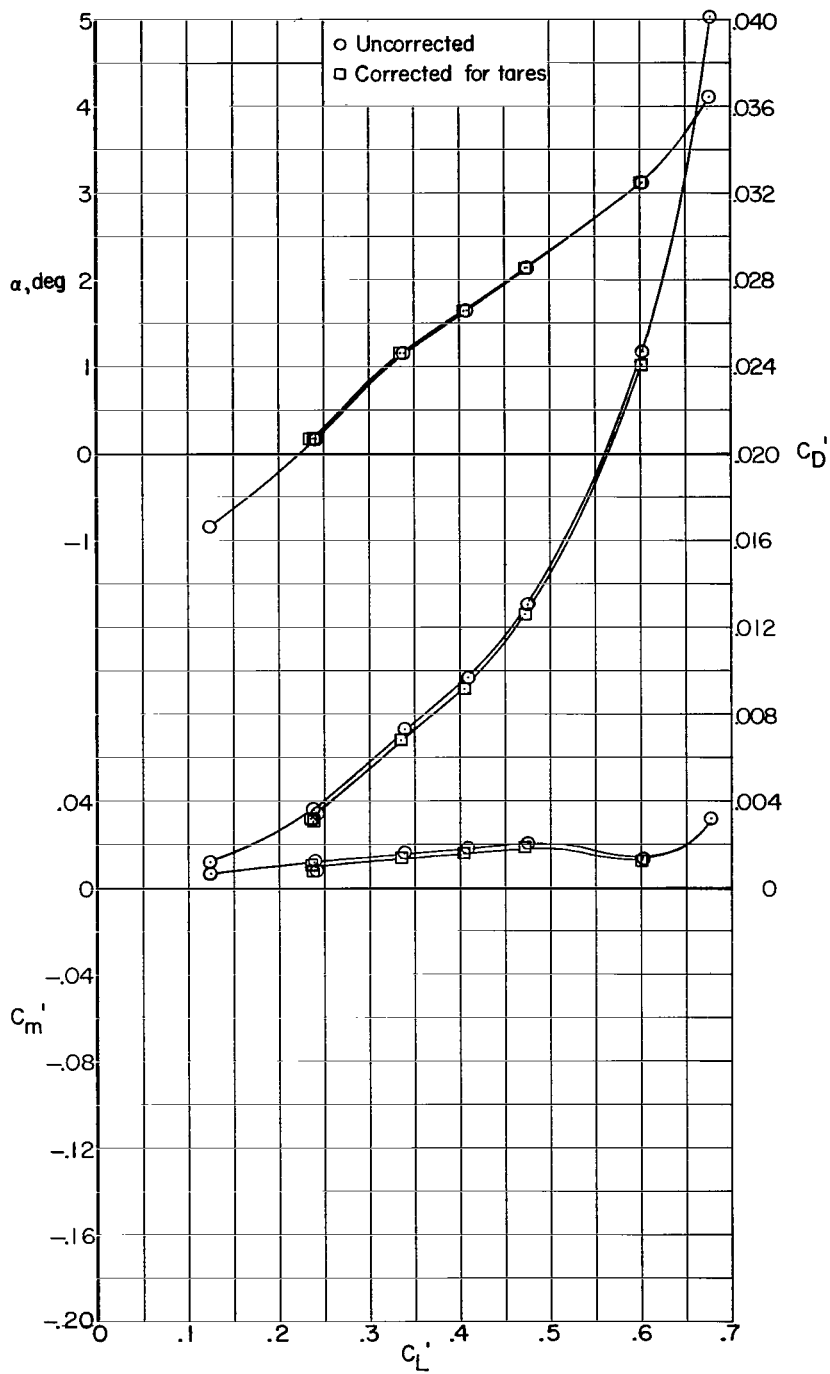
(f) $\delta_h = -1.1^\circ$; $M = 0.84$.

Figure 17.- Concluded.



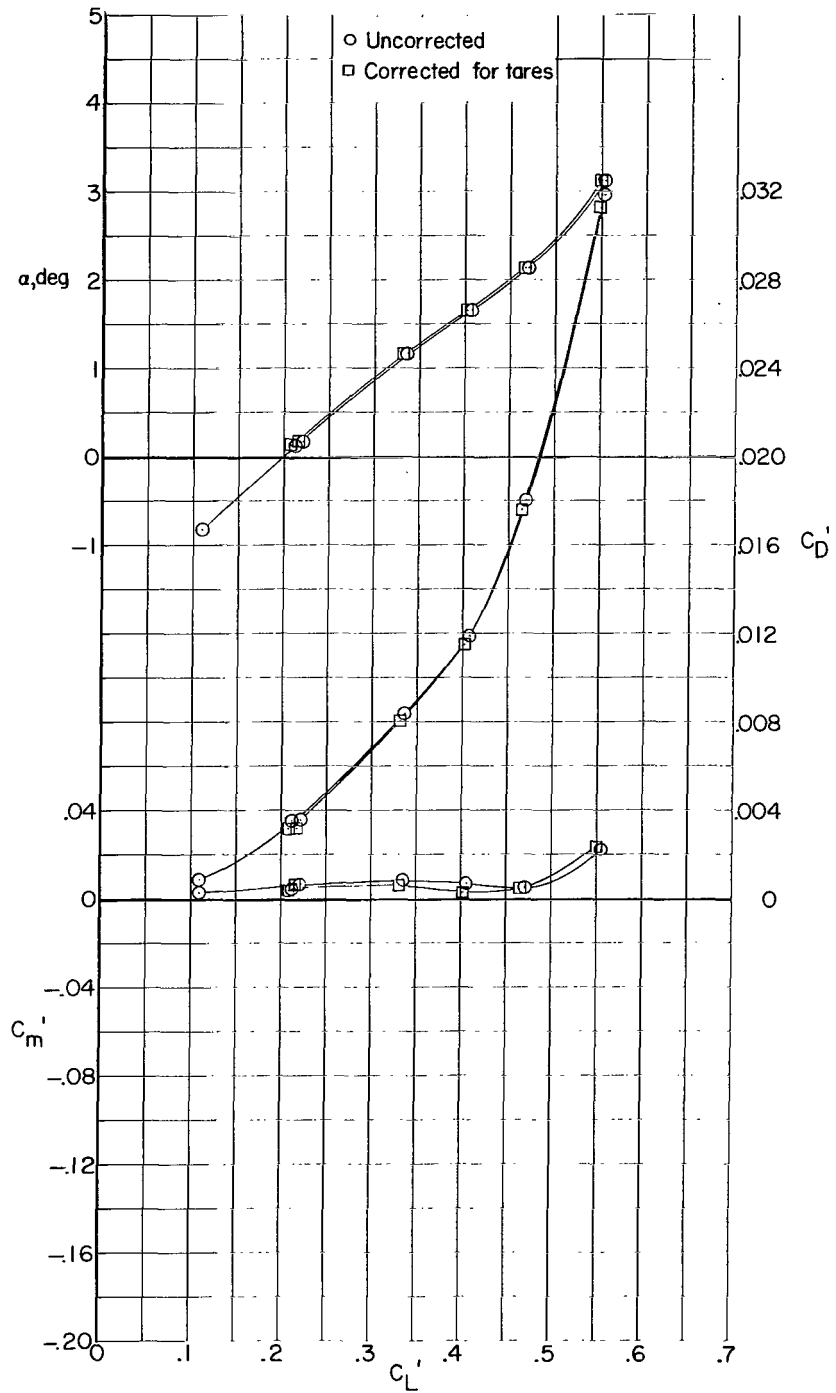
(a) Horizontal tail off; $M = 0.70$.

Figure 18.- Variation with lift coefficient of angle of attack, drag, and pitching-moment coefficients uncorrected and corrected for sting tares. Model C.



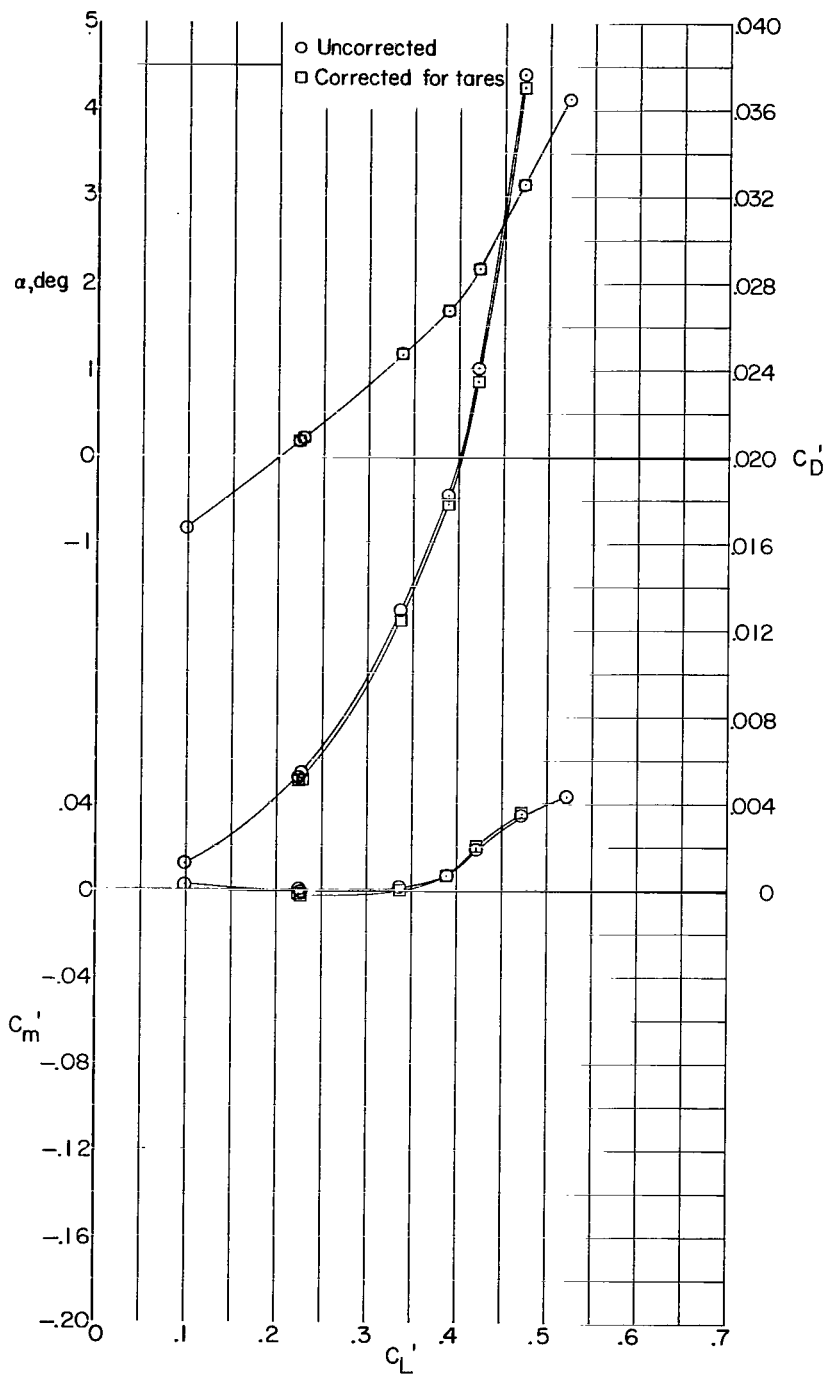
(b) Horizontal tail off; $M = 0.75$.

Figure 18.- Continued.



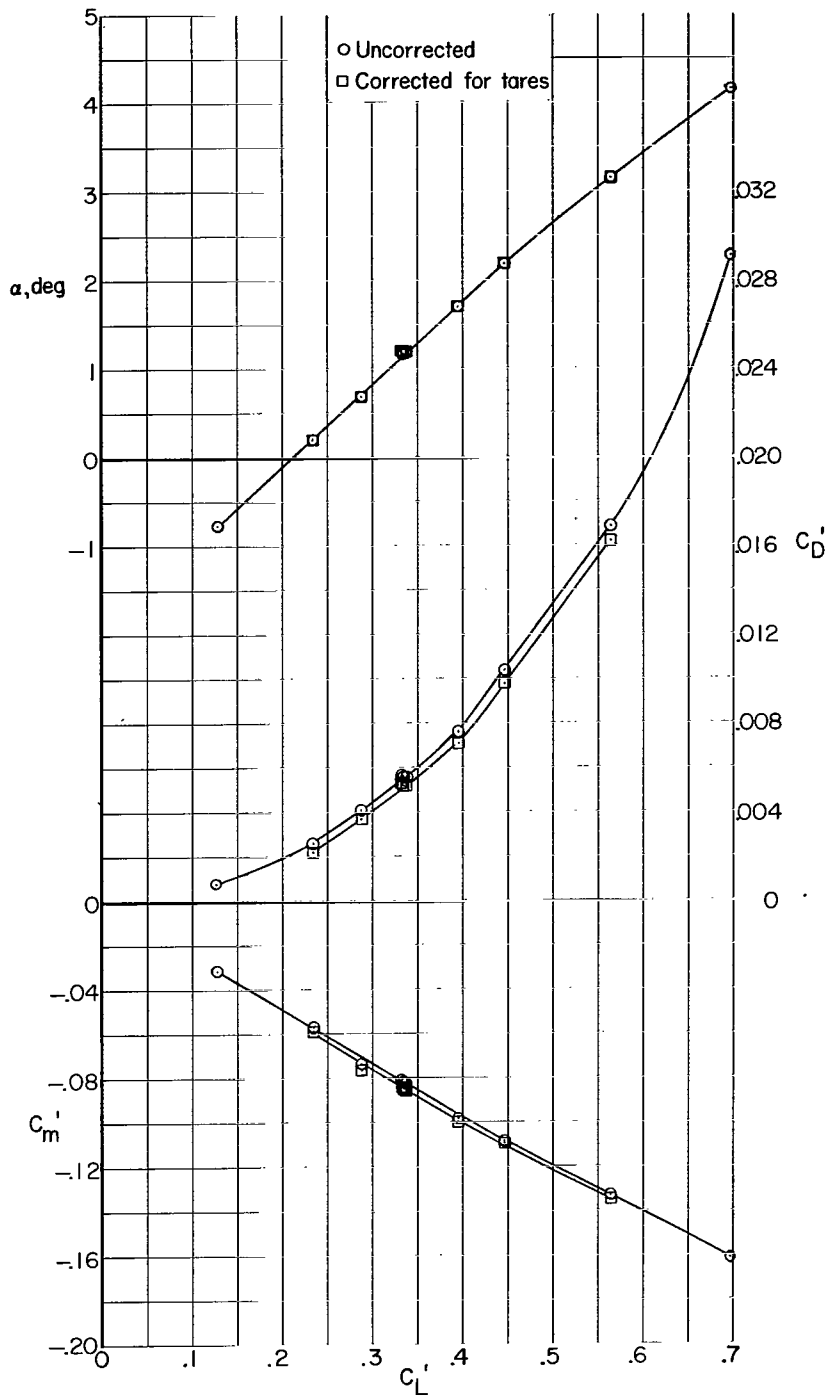
(c) Horizontal tail off; $M = 0.775$.

Figure 18.- Continued.



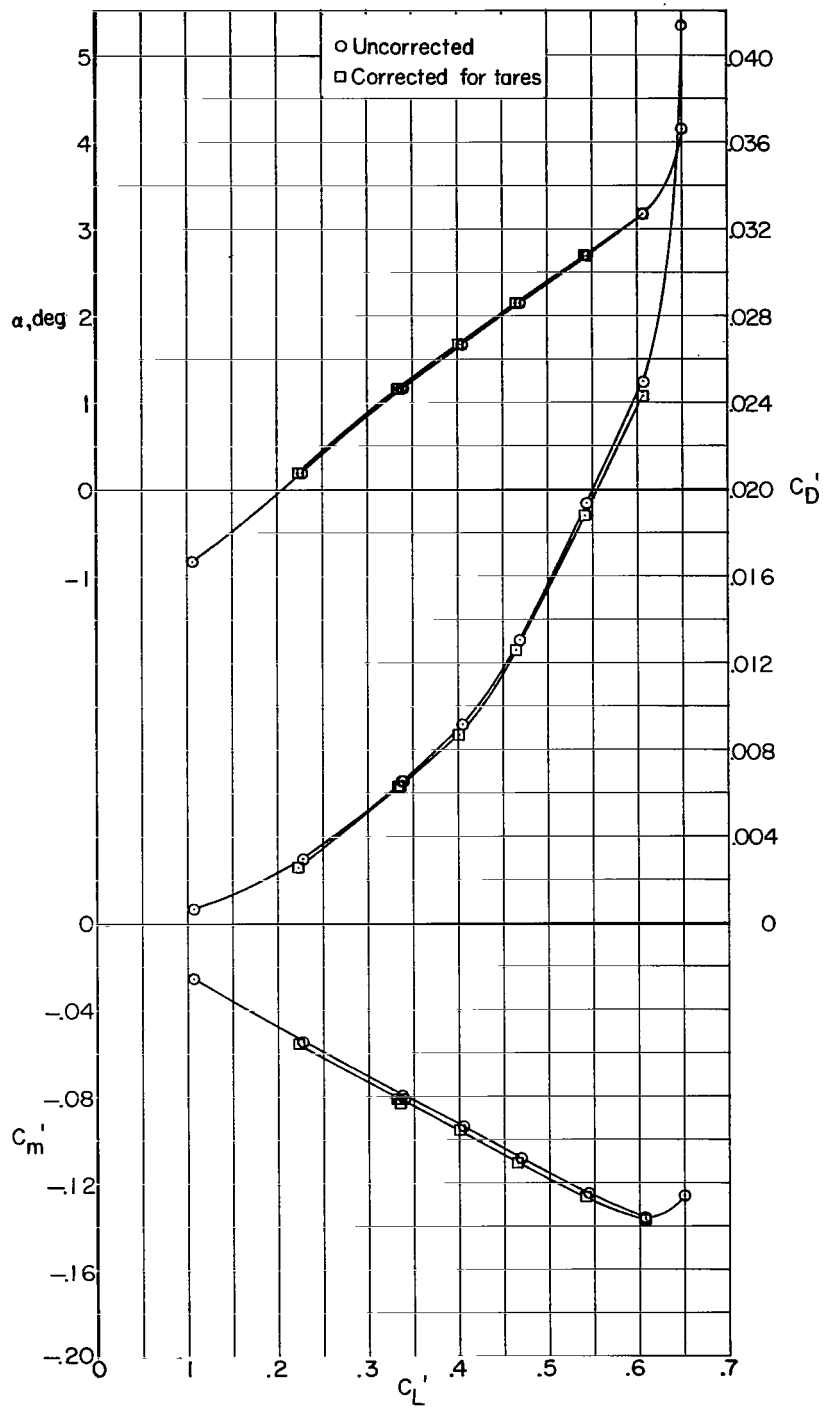
(d) Horizontal tail off; $M = 0.80$.

Figure 18.- Continued.



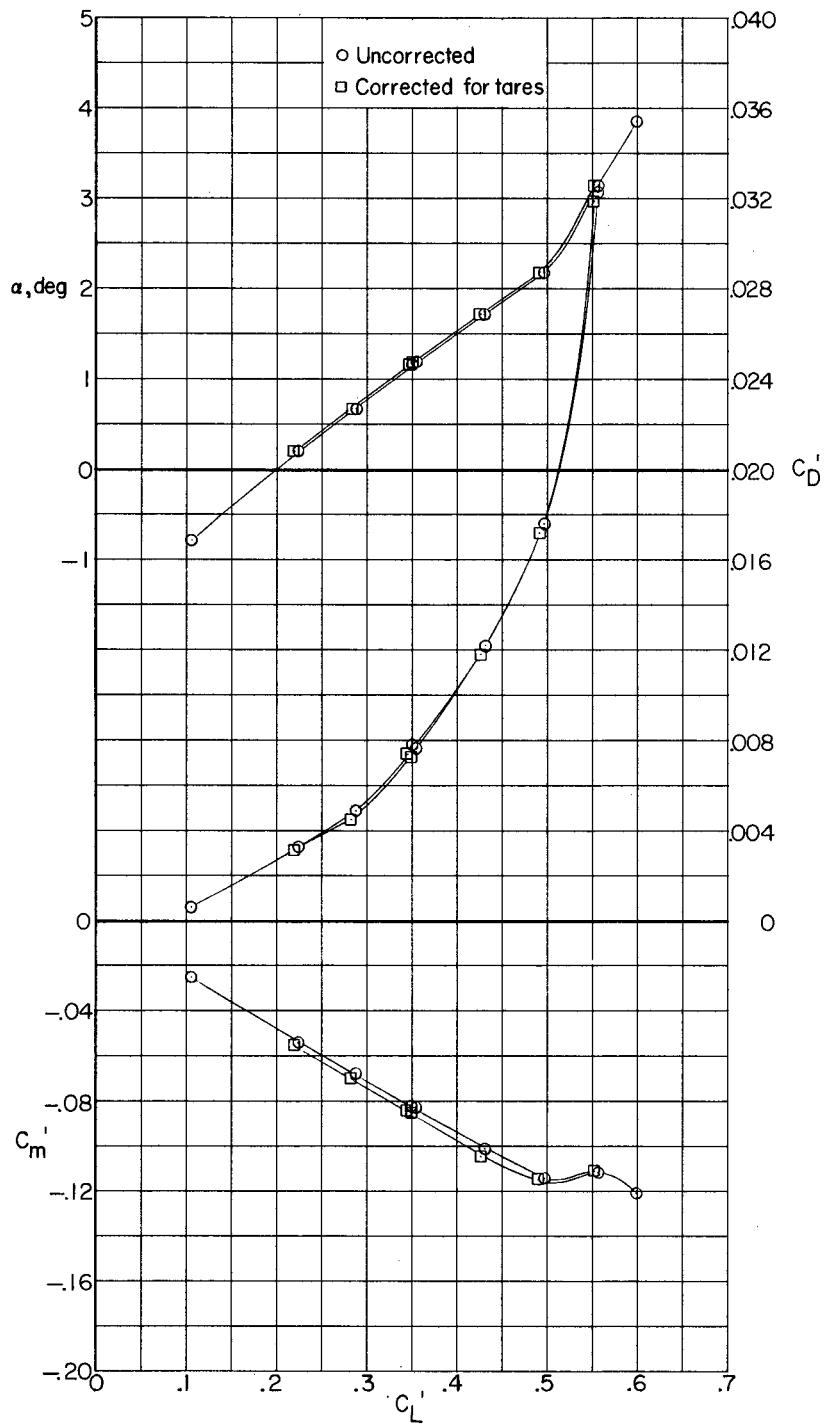
(e) $\delta_h = 0^\circ$; $M = 0.70$.

Figure 18.- Continued.



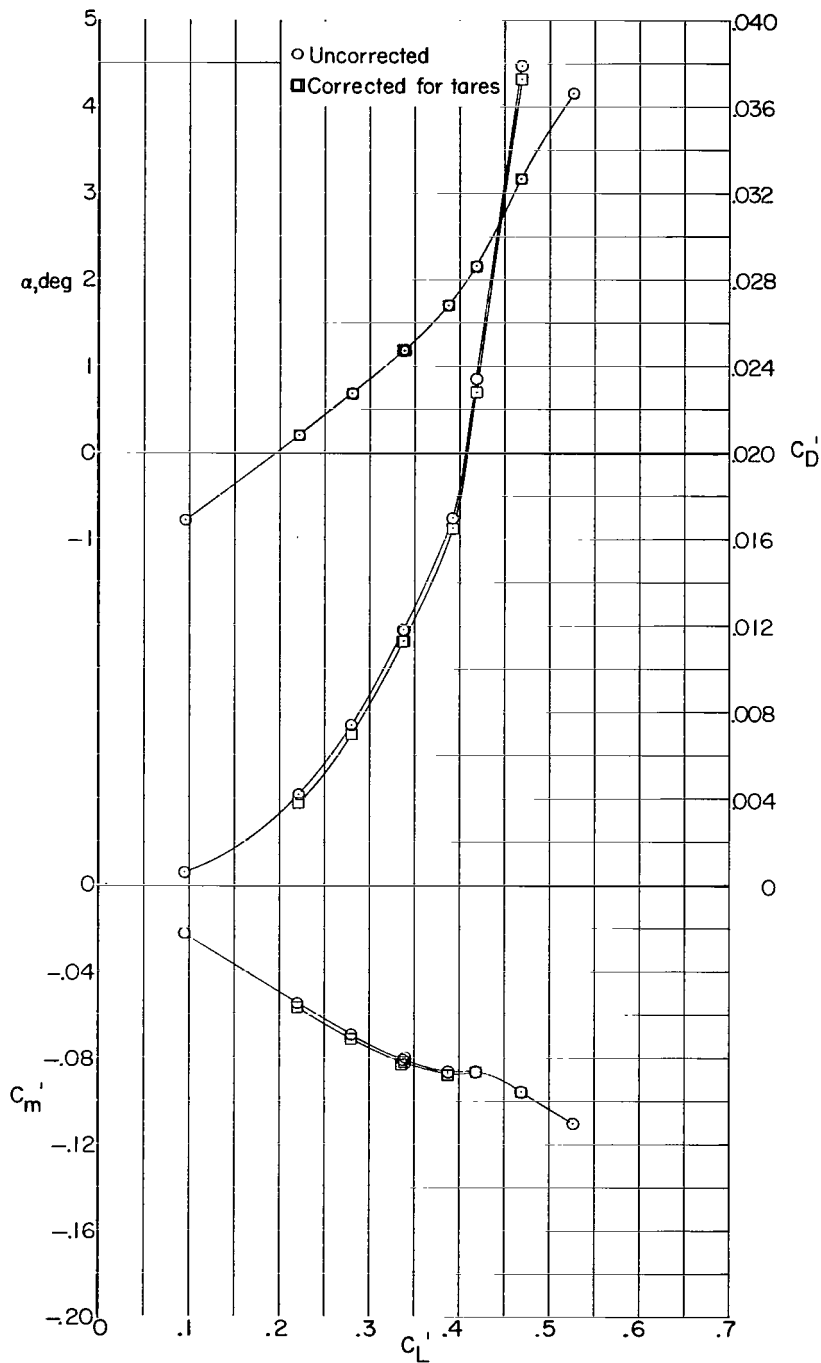
(f) $\delta_h = 0^\circ$; $M = 0.75$.

Figure 18.- Continued.



(g) $\delta_h = 0^\circ$; $M = 0.775$.

Figure 18.- Continued.



(h) $\delta_h = 0^\circ$; $M = 0.80$.

Figure 18.- Concluded.

"The aeronautical and space activities of the United States shall be conducted so as to contribute . . . to the expansion of human knowledge of phenomena in the atmosphere and space. The Administration shall provide for the widest practicable and appropriate dissemination of information concerning its activities and the results thereof."

—NATIONAL AERONAUTICS AND SPACE ACT OF 1958

NASA SCIENTIFIC AND TECHNICAL PUBLICATIONS

TECHNICAL REPORTS: Scientific and technical information considered important, complete, and a lasting contribution to existing knowledge.

TECHNICAL NOTES: Information less broad in scope but nevertheless of importance as a contribution to existing knowledge.

TECHNICAL MEMORANDUMS: Information receiving limited distribution because of preliminary data, security classification, or other reasons.

CONTRACTOR REPORTS: Scientific and technical information generated under a NASA contract or grant and considered an important contribution to existing knowledge.

TECHNICAL TRANSLATIONS: Information published in a foreign language considered to merit NASA distribution in English.

SPECIAL PUBLICATIONS: Information derived from or of value to NASA activities. Publications include conference proceedings, monographs, data compilations, handbooks, sourcebooks, and special bibliographies.

TECHNOLOGY UTILIZATION PUBLICATIONS: Information on technology used by NASA that may be of particular interest in commercial and other non-aerospace applications. Publications include Tech Briefs, Technology Utilization Reports and Notes, and Technology Surveys.

Details on the availability of these publications may be obtained from:

SCIENTIFIC AND TECHNICAL INFORMATION DIVISION
NATIONAL AERONAUTICS AND SPACE ADMINISTRATION
Washington, D.C. 20546